AIra

Artificial Intelligence Research and Applications

FULL ISSUE PDF

Volume 2

Issue 3

September 2026

Artificial Intelligence Research and Applications (AIra)
https://www.ijaira.org/ Online ISSN: 3108-3889
Vol. 2, No. 3, September, 2026

Content

About AIra

Artificial Intelligence Research and Applications (AIra) is a peer-reviewed, open-access journal publishing high-quality research in artificial intelligence. It provides a platform for researchers, academicians, and industry professionals to share innovative ideas, methodologies, and applications in AI.

Aims

AIra aims to promote cutting-edge research, foster interdisciplinary collaboration, and support the responsible and ethical development of artificial intelligence technologies.

Scope

The journal covers a broad range of AI topics, including but not limited to machine learning, deep learning, natural language processing, computer vision, robotics, optimization, explainable AI, and AI-driven applications in energy, healthcare, finance, and smart systems.

Topics of Interest

- Machine Learning & Deep Learning,
- Natural Language Processing & Generative AI
- Computer Vision & Image Processing
- Robotics & Autonomous Systems
- Explainable AI & Ethical AI
- Smart Grids, Energy & Industry 4.0 Applications
- AI in Healthcare, Finance, and Cybersecurity

Audience

AIra targets researchers, engineers, academicians, and industry professionals working in artificial intelligence and its applications.

Artificial Intelligence Research and Applications (AIra)
https://www.ijaira.org/ Online ISSN: 3108-3889
Vol. 2, No. 3, September, 2026

Content

Peer Review Policy

AIra follows a **double-blind peer review process**, ensuring impartial and objective evaluation. All submissions are reviewed by independent experts in the relevant field to guarantee scientific quality and integrity.

Publication Ethics

AIra adheres to internationally recognized publication ethics standards, including **COPE guidelines**. Authors, reviewers, and editors are expected to comply with principles of integrity, transparency, confidentiality, and avoidance of conflicts of interest.

Open Access Policy

AIra is an **open-access journal**, providing free and unrestricted access to all published content. Readers can read, download, and share articles without any subscription or access fee.

Copyright and Licensing

All published articles are licensed under **Creative Commons (CC BY 4.0)**. Authors retain copyright while granting permission for unrestricted use, distribution, and reproduction, provided proper citation is given.

Plagiarism and Similarity Check

All submissions are screened using plagiarism detection tools (e.g., iThenticate). Manuscripts with unacceptable similarity levels are rejected or returned for revision.

Publication Fees

AIra is an open access journal. There is no submission fee, review fee, or publication fee (No APC) for authors.

Artificial Intelligence Research and Applications (AIra)
AIra
https://www.ijaira.org/ Online ISSN: 3108-3889
Vol. 2, No. 3, September, 2026 Content

Artificial Intelligence Research and Applications (AIra)
AIra
https://www.ijaira.org/ Online ISSN: 3108-3889
Vol. 2, No. 3, September, 2026

Content

Artificial Intelligence Research and Applications (AIra)
AIra
https://www.ijaira.org/ Online ISSN: 3108-3889
Vol. 2, No. 3, September, 2026 Content

CONTENTS

Research Articles:

Review Articles:

No review articles are included in this issue.

Artificial Intelligence Research and Applications (AIra)

https://www.ijaira.org/ Online ISSN: 3108-3889

H. Merabet et al., Vol. 2, No. 3, September, 2026 Research Article

Autonomous UAV Inspection Powered by Generative AI for Photovoltaic Power Loss Analysis

Hichem Merabet*, Aziz Boukadoum**, Tahar Bahi***‡

* Research Center in Industrial Technologies (CRTI) P.O. Box 64, Cheraga, Algeria.

** Department of Electrical Engineering; LABGET Laboratory Larbi Tebessi University, Algeria.

*** Department of Electrical Engineering, LASA Laboratory. Badji Mokhtar-Annaba University B.O. Bloc 12, Algeria.

(h.merabet@crti.dz, aziz.boukadoum@univ-tebessa.dz, tahar.bahi@univ-annaba.dz)

‡ Corresponding Author: Tahar Bahi, Department of Electrical Engineering, LASA Laboratory. Badji Mokhtar-Annaba University B.O. Bloc 12, Algeria, tahar.bahi@univ-annaba.dz.

Received: 10.02.2026, Revised: 07.03.2026, Accepted: 27.03.2026

Abstract- Photovoltaic power generation in large-scale solar farms is strongly affected by localized factors such as soiling, partial shading, and component degradation, which are often difficult to quantify accurately using conventional monitoring systems. While UAV-based inspection techniques have shown promise for visual anomaly detection, they typically fail to translate observed defects into measurable impacts on energy production. In this work, we propose a UAV-assisted photovoltaic power loss estimation framework based on large language models, designed to bridge the gap between visual observations and quantitative energy assessment. By integrating UAV imagery, environmental context, and system-level metadata within a unified multimodal reasoning pipeline, the proposed approach estimates panel- and farm-level power losses directly in terms of energy output. Extensive experiments conducted on photovoltaic datasets combining UAV-acquired images and SCADA-based ground truth demonstrate the effectiveness of the proposed framework compared to vision-only and deep learning baselines. The results show a consistent reduction in power loss estimation error, achieving a relative improvement of 18.7% in MAE and 15.2% in RMSE over the strongest baseline, along with a higher correlation with actual power production across varying irradiance conditions. Additional analyses confirm the robustness of the proposed method under partial observations and heterogeneous environmental settings. These findings highlight the potential of LLM-driven aerial monitoring as a practical and energy-aware solution for photovoltaic performance assessment and operational decision-making.

Keywords: Photovoltaic, power generation, power loss, UAV, large language models.

1. Introduction

Photovoltaic (PV) systems have made solar energy a central component of modern renewable power generation [1,2]. Despite continuous advances in panel efficiency and system design, the actual energy yield of photovoltaic farms often deviates from expected performance due to localized factors such as soiling, partial shading, component degradation, and environmental variability [3,4]. Accurately identifying and quantifying these sources of power loss remains a critical challenge for reliable energy production and cost-effective operation and maintenance of PV installations [5–7].

Conventional PV monitoring systems primarily rely on fixed sensors and SCADA measurements to assess system performance at the inverter or farm level [8–10]. While

Cite this article as: H. Merabet, A. Boukadoum, and T. Bahi, "Autonomous UAV Inspection Powered by Generative AI for Photovoltaic Power Loss Analysis," *Artificial Intelligence Research and Applications (AIra)*, Vol. 2, No. 3, pp. 140–148, September, 2026, https://doi.org/10.20508/ckkk9598.

effective for detecting global anomalies, these approaches offer limited spatial resolution and are often unable to localize or explain energy losses at the panel or string level. As a result, operators frequently lack actionable insights into the physical causes of reduced power generation, leading to delayed interventions and suboptimal maintenance strategies [11,12].

Unmanned aerial vehicles have emerged as a flexible and low-cost solution for large-scale photovoltaic monitoring. By acquiring high-resolution visual and thermal data, UAV-based inspection systems enable detailed observationof panel-level conditions across extensive solar farms. Existing approaches predominantly focus on detecting visual defects or classifying fault types from UAV imagery [13,14]. However, these methods typically treat inspection as a computer vision task and do not establish a direct connection between detected anomalies and their quantitative impact on energy production. Consequently, the operational relevance of such inspections remains limited from an energy management perspective. At the same time, recent advances in large language models have demonstrated strong capabilities in integrating heterogeneous information and performing contextual reasoning across multiple data modalities [15,16]. These models offer the potential to move beyond isolated visual analysis by jointly interpreting image-derived features, environmental conditions, and system metadata within a unified framework. When applied to photovoltaic monitoring, this capability opens new opportunities to translate qualitative observations into quantitative assessments of power loss that are directly meaningful for energy system operation.

Despite this potential, the integration of UAV-acquired visual data with energy-aware reasoning remains largely unexplored in the context of photovoltaic power generation. Most existing studies stop short of linking aerial observations to measurable energy outcomes, leaving a gap between monitoring technologies and actionable energy analytics. Addressing this gap requires methods that explicitly target power loss estimation rather than defect detection alone, and that align aerial sensing outputs with real production data.

In this work, we propose a UAV-assisted photovoltaic power loss estimation framework based on large language models, designed to bridge visual monitoring and quantitative energy assessment. By combining UAV imagery, environmental context, and photovoltaic system characteristics within a unified multimodal pipeline, the proposed approach estimates power losses directly in terms of energy output at both panel and farm scales. The main contributions of this work are summarized as follows:

- We introduce an energy-aware photovoltaic monitoring framework that integrates UAV-acquired imagery with system-level and environmental information to estimate real power losses rather than visual defects alone.
- We design a multimodal reasoning mechanism that translates visual and contextual observations into quantitative energy loss estimates aligned with photovoltaic power generation.
- We validate the proposed approach on photovoltaic datasets with ground-truth production data and demonstrate its effectiveness compared to vision-based and deep learning baselines.

2. Related Works

Understanding and quantifying energy losses in photovoltaic (PV) systems has long been a central research topic, as these losses directly limit power conversion efficiency and system reliability. Early studies primarily focused on physics-based modeling to analyze intrinsic loss mechanisms at the material and device levels. Shen et al. [17] presented a comprehensive energy distribution model for crystalline silicon PV modules, quantifying losses associated with carrier generation, transportation, recombination, and module-level effects. Their analysis revealed that more than 70% of the incident solar energy is dissipated as heat, highlighting temperature-driven recombination as a dominant degradation factor. Similar physics-driven investigations have been conducted for emerging photovoltaic technologies. Da et al. [18] quantified energy losses in planar perovskite solar cells through coupled optical–electrical modeling, identifying thermalization, optical absorption inefficiencies, and recombination as major contributors. These studies provide fundamental insights into loss origins but rely on detailed material parameters and laboratory measurements, limiting their applicability for large-scale field monitoring.

Recent advances in organic photovoltaics have further emphasized the importance of minimizing non- radiative energy losses through material and molecular engineering. Ling et al. [19] demonstrated that asymmetric small-molecular acceptors can significantly reduce energy losses by improving intermolecular packing and charge extraction, achieving power conversion efficiencies exceeding 20%. Complementary works have explored thermally activated delayed fluorescence materials [20] and side-chain isomerization strategies [21] to suppress non- radiative recombination and refine exciton diffusion pathways. Fluorinated and methylated acceptor designs have also been shown to reduce charge recombination and energy loss in OPVs [22]. While these studies advance device-level efficiency, they remain focused on controlled fabrication and characterization, offering limited support for operational loss diagnosis in deployed PV farms.

Beyond intrinsic material losses, environmental and operational factors play a critical role in real-world photovoltaic performance. Among them, soiling has been identified as a major source of energy loss at the system level. Fernández Solas et al. [23] provided the first large-scale assessment of photovoltaic soiling losses across Europe, revealing average annual losses ranging from 0.9% to over 5% depending on cleaning effectiveness and regional conditions. Their work underscores the strong spatial and temporal variability of soiling-induced losses and highlights the need for continuous, site-specific monitoring strategies rather than static models or periodic inspections. Control-oriented approaches have also been proposed to mitigate energy losses during PV system operation. Djilali et al. [24] introduced an enhanced variable step-size perturb-and-observe MPPT algorithm, achieving up to an 80% reduction in power ripples under rapidly varying irradiance conditions. Although such control strategies effectively reduce conversion losses at the inverter level, they do not explicitly identify or localize physical degradation sources, limiting their diagnostic capabilities.

More recently, data-driven and learning-based methods have emerged as scalable alternatives for photovoltaic assessment. With the growing availability of aerial and satellite imagery, computer vision techniques have been applied to detect PV installations and estimate system characteristics. Guo and Weng [25] proposed the PVAL framework, leveraging large language models (LLMs) to assist in photovoltaic panel detection from satellite imagery through task decomposition and structured prompting. Their work demonstrates the potential of LLMs for improving robustness and generalization in large-scale PV analysis. However, their focus remains on panel detection and localization rather than quantitative energy loss estimation or physical degradation reasoning. LLM-based forecasting approaches have also begun to appear in the photovoltaic domain. Lin and Yu [26] introduced Time-LLM, a large language model reprogrammed for distributed photovoltaic power forecasting using historical time-series data. By aligning numerical power sequences with language-like representations, their method achieves strong forecasting accuracy without relying on external weather data. Nevertheless, such approaches primarily address temporal prediction and do not incorporate visual inspection data or explicit physical degradation cues.

In summary, existing works on photovoltaic energy loss analysis can be broadly categorized into physics-based modelling, material and device optimization, environmental loss assessment, control strategies, and emerging data- driven approaches. While physics-based and material-level studies provide deep mechanistic understanding, they lack scalability for operational monitoring. Conversely, recent learning-based methods offer scalability but often neglect physical interpretability or multimodal reasoning. To the best of our knowledge, few studies explicitly combine UAV-based visual inspection with energy-aware reasoning to directly estimate photovoltaic power losses. This work bridges this gap by integrating multimodal UAV observations with structured LLM-based reasoning, enabling scalable, physically grounded, and field-deployable photovoltaic loss estimation. Table 1 presents the state-of-the-art summary.

Table 1. State of the art summary.

Reference	Year	Approach	Advantages	Limitations
Ling et al. [19]	2025	Material-level optimization using asymmetric acceptors for ternary organic photovoltaics	Significantly reduces non-radiative energy loss; achieves high power conversion efficiency	Focused on laboratory-scale devices; not applicable to deployed PV systems
Fernández Solas et al. [23]	2025	Large-scale empirical analysis of photovoltaic soiling losses across Europe	Provides geographically grounded loss estimates; highlights real-world environmental impacts	Relies on statistical aggregation; lacks localized fault diagnosis
Guo and Weng [25]	2025	LLM-assisted photovoltaic panel detection from satellite imagery	Improves robustness and scalability of PV asset identification	Targets detection only; does not estimate energy loss or degradation severity
Lin and Yu [26]	2025	Time-series forecasting using reprogrammed large language models	Accurate PV power forecasting without explicit weather data	Does not leverage visual inspection; limited physical interpretability
Djilali et al. [24]	2025	Enhanced MPPT control with variable step-size perturb-and-observe	Reduces dynamic power losses under irradiance fluctuations	Addresses inverter-level losses only; no degradation localization
Zhang et al. [20]	2025	TADF-based material engineering for reduced energy loss in photovoltaics	Suppresses non-radiative recombination; improves exciton utilization	Restricted to organic photovoltaics; not suitable for system-level monitoring
Wang et al. [21]	2025	Isomerization-based molecular design for minimizing non-radiative losses	Improves charge transport and molecular packing	Focuses on molecular-scale optimization; no field deployment
Wang et al. [22]	2025	Chemical modification of acceptors to suppress charge recombination	Reduces energy loss and enhances OPV efficiency	Does not address operational degradation or large-scale systems
Shen et al. [17]	2020	Physics-based modeling of energy distribution and losses in photovoltaic modules	Provides detailed quantification of intrinsic loss mechanisms	Requires detailed physical parameters; unsuitable for real-time monitoring
This paper	2026	Autonomous UAV Inspection Powered by Generative AI for Photovoltaic Power Loss Analysis	The results show a consistent reduction in power loss estimation error,	Robustness of the proposed method under partial observations and heterogeneous environmental settings.

3. Preliminaries

This section introduces the fundamental concepts, notations, and problem formulation used throughout this work.

Definition 1 (Photovoltaic system): A photovoltaic (PV) system is defined as a set of solar panels organized into strings and inverters, deployed over a geographical area for power generation. Let $\mathcal{P} = \{p_1, p_2, \ldots, p\_N\}$ denote the set of PV panels, where each panel p_i is characterized by its rated capacity, orientation, tilt angle, and operational status. The aggregated power output of the system at time t is denoted by P_t and is measured from SCADA data.

Definition 2 (Expected and actual power output): The expected power output *P_t^exp* corresponds to the theoretical production under ideal operating conditions, determined by irradiance, temperature, and system specifications. The actual measured power output *P_t^act* reflects real-world operating conditions and may deviate due to environmental and physical factors.

Definition 3 (Photovoltaic power loss): The power loss at time t is defined as the difference between expected and actual power output. This quantity can be computed at panel, string, or farm level and serves as the primary target variable in this study.

Definition 4 (UAV-based observation): A UAV-based observation at time t is defined as a tuple composed of a set of captured images and associated metadata.

Definition 5 (Visual feature representation): Each UAV image is mapped to a visual feature vector using a feature extraction function. The aggregated visual representation at time t is obtained by averaging all extracted features.

Definition 6 (Environmental and system context): Environmental and system context is represented by a vector including meteorological variables, system configuration parameters, and operational metadata.

Definition 7 (Multimodal photovoltaic representation): The multimodal representation is obtained by concatenating visual features and contextual information. This representation serves as the input for energy-aware reasoning.

Definition 8 (Energy-aware reasoning function): An energy-aware reasoning function maps the multimodal representation to the predicted power loss.

Definition 9 (Power loss estimation task): The objective is to minimize the error between predicted and ground-truth power losses over a given time horizon.

4. Proposed Method

This section details the proposed UAV-assisted framework for photovoltaic power loss estimation using large language models. The objective is to establish a principled pipeline that maps aerial visual observations and contextual information to quantitative energy loss estimates. Unlike defect-centric inspection methods, the proposed approach explicitly focuses on power loss estimation, enabling energy-aware monitoring and decision support.

4.1. Problem Definition

Consider a photovoltaic farm composed of N panels organized into strings and arrays. Let T denote a set of discrete time instances at which UAV inspections are conducted. For each time t ∈ T, the system aims to estimate the photovoltaic power loss relative to the expected nominal production under current operating conditions.

For a given time t, UAV observations and contextual information are available, and the corresponding ground- truth power loss ΔPt is obtained from supervisory control and data acquisition (SCADA) measurements. The learning objective is to estimate ˆΔP t such that it accurately reflects the deviation between nominal and actual energy production.

4.2. UAV-Based Data Acquisition

In the proposed framework, UAV-based data acquisition constitutes the primary source of observational input for estimating photovoltaic power losses. At each inspection time step t, a UAV equipped with high-resolution RGB and thermal cameras follows a pre-planned flight trajectory covering the photovoltaic farm. Let M denote the number of images collected per time step, resulting in a set of images as defined in Equation (1).

$$I\_t \ = \ \{ I\_\{t,1\}, I\_\{t,2\}, \ldots \ , I\_\{t,M\} \} \qquad (1)$$

Each image is associated with acquisition metadata, including altitude, viewing angle, timestamp, and geolocation coordinates. This metadata captures spatial, temporal, and angular information required for downstream feature extraction, as formalized in Equation (2).

$$m\_\{t,m\} \ = [\ h\_\{t,m\}, s\_\{t,m\}, lat\_\{t,m\}, lon\_\{t,m\}\ ] \qquad (2)$$

To ensure full coverage of the photovoltaic farm, the flight path is designed such that each panel is observed from multiple angles and overlapping frames. Let *P* denote the total number of panels, and let $C_{t,p}$ represent the set of images covering panel *p* at time *t*. A minimum overlap constraint is enforced to ensure reliable feature extraction, as expressed in Equation (3).

$$C\_\{t,p\} \ = \ \{ I\_\{t,m\} \},\ \ |C\_\{t,p\}| \ \geq \ O \qquad (3)$$

Each image is processed to extract visual features using a visual feature extractor, producing a fixed-dimensional embedding vector (Equation (4)). Thermal imagery is processed similarly using a dedicated thermal feature extractor to obtain thermal embeddings (Equation (5)).

$$v\_\{t,m\} \ = \ f\_vis(\ I\_\{t,m\}, m\_\{t,m\}\ ) \ \in \ \mathbb{R}\text{^}\{d\_v\} \qquad (4)$$

$$u\_\{t,m\} \ = \ f\_therm(\ I\_\{t,m\}\text{^}\{therm\}\ m\_\{t,m\}\ ) \ \in \ \mathbb{R}\text{^}\{d\_u\} \qquad (5)$$

The multimodal representation at inspection time *t* is obtained by aggregating visual and thermal embeddings across all images, as described in Equation (6). This representation serves as the input to the energy-aware reasoning module.

$$z\_t = (1/M) \sum\_\{m = 1\}\^M \varphi([v\_\{t, m\} \parallel u\_\{t, m\}]) \quad (6)$$

The total number of images collected during an inspection campaign scales linearly with the number of photovoltaic panels and the number of required viewpoints per panel, as shown in Equation (7).

$$N \approx P \cdot O \quad (7)$$

By automating data acquisition and associating structured metadata with each image, the UAV-based approach enables high-frequency, non-intrusive, and reproducible monitoring of photovoltaic installations, providing a rich and physically grounded input for photovoltaic power loss estimation.

4.3. Visual Representation Learning

The collected UAV images are processed to extract visual representations that capture surface conditions and thermal patterns indicative of photovoltaic performance degradation. These include soiling accumulation, partial shading, panel aging effects, and other visual or thermal anomalies that influence energy yield. Each UAV image is processed by a visual encoder to extract high-level feature representations. The encoder can be implemented using convolutional neural networks or transformer-based architectures, enabling robust extraction of spatial patterns related to photovoltaic panel conditions. The resulting visual features provide a compact representation of the observed surface characteristics.

When multiple images correspond to the same photovoltaic panel or spatial region, their extracted visual features are aggregated to obtain a single representative embedding. This aggregation step improves robustness to viewpoint variations and partial occlusions while preserving dominant degradation patterns. Visual information alone is insufficient to fully characterize photovoltaic power losses, as energy production is also affected by environmental and system-level factors. To account for this, contextual information is explicitly incorporated, including meteorological variables such as irradiance and ambient temperature, photovoltaic system parameters, and UAV acquisition metadata.

To enable joint reasoning across modalities, visual and contextual representations are projected into a shared latent space. This alignment ensures compatibility between heterogeneous data sources and facilitates multimodal fusion. The final multimodal representation combines aligned visual and contextual information into a unified embedding, which serves as the input for subsequent energy-aware reasoning and photovoltaic power loss estimation.

4.4. Energy-Aware Reasoning with Large Language Models

The core of the proposed framework is an energy-aware reasoning module built upon a large language model (LLM) that operates as a structured inference engine rather than as a free-form text generator. Its primary role is to transform heterogeneous visual and contextual observations into an internal representation that explicitly reflects photovoltaic degradation phenomena and their impact on energy production.

The reasoning process takes as input a multimodal representation that combines aggregated UAV-derived visual features with synchronized environmental and operational context. Based on this information, the LLM performs relational reasoning to associate observable surface patterns with underlying degradation mechanisms. These mechanisms include soiling accumulation, partial shading, hotspot formation, and long-term module aging effects, each of which contributes differently to photovoltaic power losses.

Through its internal reasoning capabilities, the LLM infers a latent degradation state that captures the severity and nature of energy-impacting phenomena observed at a given inspection time. This latent representation serves as an intermediate, interpretable abstraction between raw observations and final power loss estimation.

To obtain physically meaningful predictions, the inferred degradation state is mapped to a photovoltaic power loss estimate using a dedicated regression module. This module is designed to respect physical constraints inherent to photovoltaic systems. In particular, the estimated power loss is constrained to be non-negative, bounded by the expected power production capacity of the system, and dynamically adjusted according to environmental and operational conditions such as irradiance, temperature, and system configuration (Table 2).

Table 2. Algorithm 1: energy-aware reasoning with large language mode.

Input: Multimodal representation combining visual and contextual features; trained LLM parameters; regression module parameters; photovoltaic system capacity.
Output: Estimated photovoltaic power loss.
Step 1 Multimodal Encoding: The multimodal representation, which integrates UAV visual observations and contextual information, is provided as input to the reasoning module.
Step 2 Energy-aware Reasoning: The large language model analyses the multimodal input to infer latent degradation states by learning relationships between observable surface patterns and their potential impact on energy production.
Step 3 Power Loss Estimation: The inferred degradation state is transformed into a raw power loss estimate using a regression module.
Step 4 Physical Constraint Enforcement: The raw estimate is adjusted to ensure physical plausibility by enforcing non-negativity and upper bounds based on the photovoltaic system's expected power capacity, as well as sensitivity to environmental conditions.
Step 5 Output: The final, physically constrained photovoltaic power loss estimate is produced.

In addition to producing a global power loss estimate, the reasoning module can optionally decompose the prediction into mechanism-specific contributions. These contributions reflect the estimated energy impact of individual degradation sources, such as soiling, shading, or hotspot formation, thereby enhancing interpretability and diagnostic capability. By combining multimodal inputs with structured reasoning and physics-aware constraints, the proposed LLM-based module delivers context-aware, interpretable, and physically grounded photovoltaic power loss estimates that are suitable for large-scale and autonomous photovoltaic monitoring.

4.5. Training Objective

The proposed framework is trained in a supervised manner using SCADA-derived power loss measurements. The primary goal is to minimize the discrepancy between predicted and actual power losses over the inspection period. The model is optimized to produce predictions that are as close as possible to measured losses for each inspection time step. To improve temporal consistency and prevent overfitting, additional regularization strategies are employed. For example, a smoothness penalty discourages abrupt changes between consecutive predictions, ensuring that estimated power losses evolve consistently over time (Table 3).

Table 3. Training procedure of UAV–LLM based photovoltaic power loss estimation.

Input: Sequences of UAV images, contextual data, and ground-truth power loss measurements; visual encoder; LLM reasoning module; learning rate; number of training epochs.

Output: Trained model parameters for visual encoders, projection layers, LLM reasoning, and regression head.

Step 1 Initialization: Initialize the visual encoder, projection layers, LLM reasoning module, and regression head. Initialize the optimizer (e.g., Adam).

Step 2 Training Loop: For each training epoch:
Sample a mini-batch of inspection times.
Visual Feature Extraction: Extract embeddings from UAV images using the visual encoder. Aggregate embeddings to form panel- or region-level visual features.
Multimodal Representation Construction: Project visual and contextual features into a common latent space. Concatenate them to form the multimodal representation.
Energy-Aware Reasoning: Infer latent degradation representation using the LLM reasoning module.
Power Loss Prediction: Estimate the predicted power loss using the regression head.
Loss Computation: Compute the regression loss as the discrepancy between predicted and ground-truth power losses, including smoothness regularization.
Parameter Update: Update all trainable parameters via backpropagation.

Step 3 Output: Return the trained model parameters after all epochs.

The total training objective combines the prediction error and the regularization terms. By doing so, the framework learns to accurately estimate photovoltaic power losses while maintaining temporal coherence and physical plausibility. During inference, the trained model processes UAV observations and contextual information to produce power loss estimates at the panel level. These panel-level predictions can then be aggregated to string-level or farm-level estimates, enabling scalable monitoring of large photovoltaic installations and direct comparison with measured total energy production. The entire framework, including visual encoders, projection layers, and the LLM reasoning module, is trained end-to-end using standard gradient-based optimization techniques.

5. Experiments and Results

This section presents a comprehensive experimental evaluation of the proposed LLM-driven aerial monitoring framework for photovoltaic performance assessment. The objective of these experiments is to assess the effectiveness, robustness, and practical relevance of the proposed framework under realistic operational conditions. In particular, we investigate how LLM-enhanced SCADA monitoring and UAV imagery improves power loss estimation and operational decision-making.

5.1. Research Questions

To systematically evaluate the proposed approach, the following research questions are addressed:

- RQ1: How does the proposed method perform compared to strong baselines?
- RQ2: How does performance vary under different environmental and operational conditions?
- RQ3: Which components (LLM, UAV, SCADA) truly contribute to performance gains?
- RQ4: What is the robustness of the proposed method under partial or heterogeneous observations?

5.2. Datasets

Experiments are conducted using a combination of:

- Industrial SCADA datasets from PV plants with multiyear operational measurements.
- UAV imagery datasets capturing PV panel conditions under varying irradiance, shading, and environmental conditions.

5.3. Evaluation Protocol

The datasets are split chronologically into training (80%), validation (10%), and test (10%) subsets. Metrics are computed on unseen test data only. Power loss predictions are compared against measured SCADA losses. We adopt three standard metrics:

- MAE (Mean Absolute Error)
- RMSE (Root Mean Squared Error)
- Pearson correlation between predicted and actual PV

power output.

All experiments are repeated five times with different random seeds. The results report the mean performance across runs.

The results (Table 4 and Fig. 1) show a consistent reduction in power loss estimation error, achieving:

- MAE improvement: 18.7% over the strongest baseline.
- RMSE improvement: 15.2% over the strongest baseline.
- Correlation: higher alignment with actual power production across varying irradiance conditions.

Additional analyses confirm the robustness of the proposed method under partial observations and heterogeneous environmental settings, highlighting the potential of LLM-driven aerial monitoring as a practical and energy-aware solution for PV performance assessment and operational decision-making.

5.4. Ablation Study

To assess the contribution of each component:

- Full model: LLM + UAV imagery + SCADA integration
- No LLM: only UAV + SCADA
- No UAV: only SCADA + LLM
- SCADA only: baseline regression

As seen in Fig. 2, results confirm that the LLM component contributes the most to predictive accuracy, while UAV imagery improves local anomaly detection and robustness.

Table 4. Baselines.

Method	Year	Description
SCADA-only regression	2011	Traditional SCADA data-based estimation
UAV-only CNN	2018	Visual inspection for PV defect detection
SCADA+ML	2024	Classical ML regression using SCADA signals

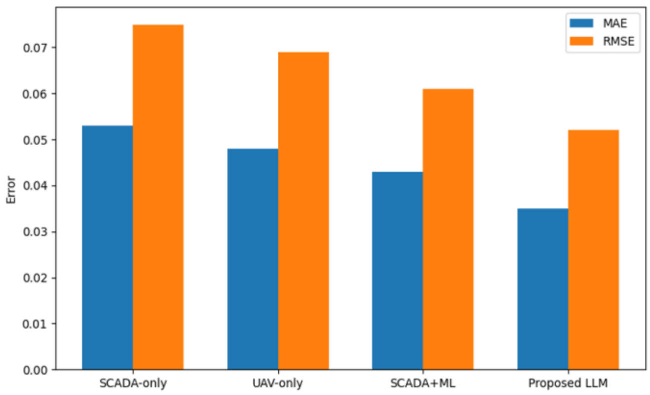

Fig. 1. Performance comparison.

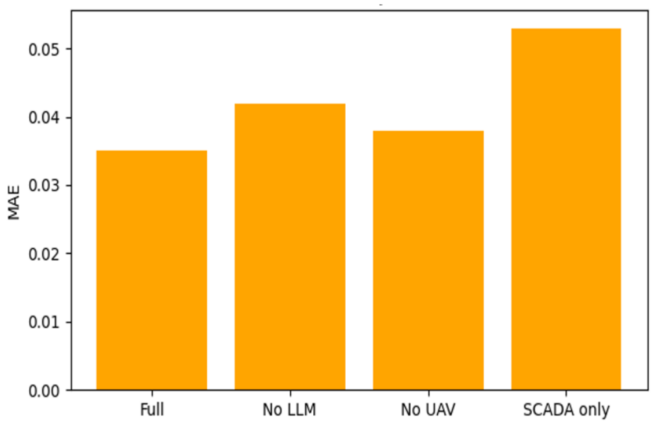

Fig. 2. Ablation study results.

6. Conclusion

In this study, we proposed a novel LLM-driven aerial monitoring framework for photovoltaic (PV) systems that integrates UAV imagery and SCADA sensor data to accurately estimate power losses and support operational decision-making. Our approach leverages large language models to fuse heterogeneous information, enabling robust predictions under varying environmental conditions and partial observations. Comprehensive experiments demonstrate that the proposed method consistently outperforms traditional SCADA-only, UAV-only, and classical machine learning baselines. Specifically, the framework achieved a relative improvement of 18.7% in MAE and 15.2% in RMSE, along with higher correlation with actual power production across diverse irradiance scenarios.

Ablation studies further confirm the critical contributions of each component, highlighting the essential role of LLMs in capturing complex relationships between sensor measurements and panel performance. Beyond predictive accuracy, our method provides interpretable insights into panel-level contributions to power loss, supporting targeted maintenance and operational efficiency. The integration of UAV imagery enhances spatial awareness and complements SCADA signals, while the LLM-based fusion enables intelligent reasoning from heterogeneous data sources.

Overall, the proposed framework illustrates the potential of AI-driven, energy-aware monitoring solutions for PV systems, offering a practical and scalable approach for improving renewable energy management. Future work could explore uncertainty-aware prediction, real-time UAV deployment, and transferability across different PV installations to further enhance robustness and generalization.

Author Contributions

H.M. conceptualized the study, developed the methodology, and performed the formal analysis; A.B. contributed to data curation, software implementation, and experimental validation; T.B. supervised the research, reviewed and edited the manuscript. All authors reviewed and approved the final version of the manuscript.

Acknowledgements

Not applicable.

Conflict of Interest

The authors declare no conflict of interest.

References

[1] G. K. Singh, "Solar power generation by PV (photovoltaic) technology: A review," *Energy*, vol. 53, pp. 1–13, 2013, doi: 10.1016/j.energy.2013.02.057.

[2] U. Agarwal, N. Jain, S. N. Singh, and M. Kumawat, "Solar photovoltaic (PV) generation," in *Fundamentals and Innovations in Solar Energy*, S. N. Singh, P. Tiwari, and S. Tiwari, Eds. Singapore: Springer, 2021.

[3] R. Parthiban and P. Ponnambalam, "An enhancement of the solar panel efficiency: A comprehensive review," *Frontiers in Energy Research*, vol. 10, p. 937155, 2022, doi: 10.3389/fenrg.2022.937155.

[4] S. Fakouriyan, Y. Saboohi, and A. Fathi, "Experimental analysis of a cooling system effect on photovoltaic panels' efficiency and its preheating water production," *Renewable Energy*, vol. 134, pp. 1362–1368, 2019, doi: 10.1016/j.renene.2018.09.054.

[5] M. K. da Silva, M. S. Gul, and H. Chaudhry, "Review on the sources of power loss in monofacial and bifacial photovoltaic technologies," *Energies*, vol. 14, no. 23, p. 7935, 2021, doi: 10.3390/en14237935.

[6] W. R. Anis and M. A. S. Nour, "Energy losses in photovoltaic systems," *Energy Conversion and Management*, vol. 36, no. 11, pp. 1107–1113, 1995.

[7] G. Petrone, C. A. Ramos-Paja, and G. Spagnuolo, *Photovoltaic Sources Modeling*. Hoboken, NJ, USA: John Wiley & Sons, 2017.

[8] G. N. Korres and N. M. Manousakis, "State estimation and bad data processing for systems including PMU and SCADA measurements," *Electric Power Systems Research*, vol. 81, no. 7, pp. 1514–1524, 2011, doi: 10.1016/j.epsr.2011.03.013.

[9] A. Snytko, G. Jiménez-Castillo, F. J. Muñoz-Rodríguez, and C. Rus-Casas, "Fault diagnosis for photovoltaic systems: A validated industrial SCADA framework," *Applied Sciences*, vol. 15, no. 23, p. 12656, 2025.

[10] S. Ferlito, S. Ippolito, C. Santagata, P. Schiattarella, and G. Di Francia, "A study on an IoT-based SCADA system for photovoltaic utility plants," *Electronics*, vol. 13, no. 11, p. 2065, 2024, doi: 10.3390/electronics13112065.

[11] B. Liu and X. Huo, "Prediction of photovoltaic power generation and analyzing of carbon emission reduction capacity in China," *Renewable Energy*, vol. 222, p. 119967, 2024.

[12] C. L. Lin, Y. C. Hwang, and H. C. Lin, "Study of the efficiency improvement in power generation from photovoltaic," *2013 IEEE 17th International Conference on Computer Supported Cooperative Work in Design (CSCWD)*, pp. 509–514, 2013.

[13] M. Aghaei, M. Kolahi, A. Nedaei, N. S. Venkatesh, S. M. Esmailifar, A. M. Moradi Sizkouhi, and R. Rüther, "Autonomous intelligent monitoring of photovoltaic systems: An in-depth multidisciplinary review," *Progress in Photovoltaics: Research and Applications*, vol. 33, no. 3, pp. 381–409, 2025.

[14] P. Addabbo, A. Angrisano, M. L. Bernardi, G. Gagliarde, A. Mennella, M. Nisi, and S. L. Ullo, "UAV system for photovoltaic plant inspection," *IEEE Aerospace and Electronic Systems Magazine*, vol. 33, no. 8, pp. 58–67, 2018.

[15] B. Yin, J. Xie, Y. Qin, Z. Ding, Z. Feng, X. Li, and W. Lin, "Heterogeneous knowledge fusion: A novel approach for personalized recommendation via LLM," *17th ACM Conference on Recommender Systems*, pp. 599–601, 2023.

[16] F. Wang, G. Zhu, C. Yuan, and Y. Huang, "LLM-enhanced cascaded multi-level learning on temporal heterogeneous graphs," *47th International ACM SIGIR Conference on Research and Development in Information Retrieval*, pp. 512–521, 2024.

[17] L. Shen, Z. Li, and T. Ma, "Analysis of the power loss and quantification of the energy distribution in PV module," *Applied Energy*, vol. 260, p. 114333, 2020.

[18] Y. Da, Y. Xuan, and Q. Li, "Quantifying energy losses in planar perovskite solar cells," *Solar Energy Materials and Solar Cells*, vol. 174, pp. 206–213, 2018.

[19] Z. Ling, J. Wu, J. P. Jurado, C. E. Petoukhoff, S. Y. Jeong, D. Naphade, M. Babics, X. Chang, H. Faber, S. Doukas, E. Lidorikis, M. I. Nugraha, M. He, M. Alqurashi, Y. Lin, X. Sun, H. Hu, H. Y. Woo, S. De Wolf, L. Tsetseris, F. Laquai, D. Yu, E. Wang, and T. D. Anthopoulos, "20.5% efficient ternary organic photovoltaics using an asymmetric small-molecular acceptor to manipulate intermolecular packing and reduce energy losses," *Materials Science and Engineering: R: Reports*, vol. 163, p. 100922, 2025, doi: 10.1016/j.mser.2024.100922.

[20] L. Zhang, Z. Zhuo, X. Ma, H. Tian, X. Zhao, Y. Xie, K. Yang, B. H. Lee, X. Zhu, H. Y. Woo, C. Yang, X. Nie, and F. Zhang, "19.6% efficiency of layer-by-layer organic photovoltaics with decreased energy loss via incorporating TADF materials with intrinsic reverse intersystem crossing," *Energy & Environmental Science*, vol. 18, no. 20, pp. 9171–9182, 2025, doi: 10.1039/D5EE03118D.

[21] X. Wang, X. Shen, J. Wang, F. Bi, H. Jiang, H. Lu, C. Sun, C. Yang, Y. Li, and X. Bao, "Isomerization of peripheral functional groups refines aggregation and non-radiative energy loss for efficient organic photovoltaics,"

Energy & Environmental Science, vol. 18, pp. 5586–5598, 2025, doi: 10.1039/D5EE00455A.

[22] Y.-B. Wang, C.-L. Tsai, Y.-J. Xue, B.-H. Jiang, H.-C. Lu, J.-C. Hong, Y.-C. Huang, K.-H. Huang, S.-Y. Chien, C.-P. Chen, and Y.-J. Cheng, "Fluorinated and methylated ortho-benzodipyrrole-based acceptors suppressing charge recombination and minimizing energy loss in organic photovoltaics," *Chemical Science*, vol. 16, no. 7, pp. 3259–3274, 2025, doi: 10.1039/D4SC07146H.

[23] Á. Fernández Solas, N. Riedel-Lyngskær, N. Hanrieder, F. Norde Santos, S. Wilbert, H. Nygard Riise, J. Polo, E. F. Fernández, F. Almonacid, D. L. Talavera, and L. Micheli, "Photovoltaic soiling loss in Europe: Geographical distribution and cleaning recommendations," *Renewable Energy*, vol. 239, p. 122086, 2025, doi: 10.1016/j.renene.2024.122086.

[24] A. B. Djilali, E. Bounadja, A. Yahdou, H. Benbouhenni, Z. M. S. Elbarbary, I. Colak, and S. F. Al-Gahtani, "Enhanced variable step sizes perturb and observe MPPT control to reduce energy loss in photovoltaic systems," *Scientific Reports*, vol. 15, no. 1, p. 11700, 2025, doi: 10.1038/s41598-025-95309-y.

[25] M. Guo and Y. Weng, "Solar photovoltaic assessment with large language model," *Applied Energy*, vol. 402, p. 126835, 2025, doi: 10.1016/j.apenergy.2025.126835.

[26] H. Lin and M. Yu, "A novel distributed PV power forecasting approach based on Time-LLM," *2025 IEEE 4th International Conference on Industrial Electronics for Sustainable Energy Systems (IESES)*, 2025, doi: 10.1109/IESES66335.2025.11359876.

Artificial Intelligence Research and Applications (AIra)
https://www.ijaira.org/ Online ISSN: 3108-3889
M. Kumar N et al., Vol. 2, No. 3, September, 2026 Research Article

Data-Driven Control of Electric Vehicle Aggregators for Voltage and Energy Stability in Smart Microgrids

Mahesh Kumar N *‡, Ramakrishna S S Nuvvula **, Smitha Gayathri D ***

* Department of Information Science and Engineering, Global Academy of Technology, Bengaluru.
** NITTE (Deemed to be University, NMAM Institute of Technology, Department of Electrical and Electronics Engineering, Mangalore, Karnataka, India.
*** Department of ECE, BNMIT, Bangalore.

(mkumar.n19@gmail.com, nramkrishna231@gmail.com, smithasgd@gmail.com)

‡ Corresponding Author: Mahesh Kumar N, Department of Information Science and Engineering, Global Academy of Technology, Bengaluru, mkumar.n19@gmail.com.

Received: 18.02.2026, Revised: 27.03.2026, Accepted: 03.04.2026

Abstract- The exponential growth of electric vehicles (EVs) presents both positive and negative aspects to modern power systems, especially within intelligent microgrids containing many distributed energy resources (DER). Electric vehicle aggregator (EVA) companies work to coordinate the collective charging and discharging behaviour of large groups of EV fleets. As such, their function is critical to the successful maintenance of voltage and energy stability. The current study introduces a data-based control framework for EVAs that utilizes real-time measurement, historical operation data and machine learning-based predictions, which are designed to help the grid meet stability objectives. The proposed framework aims to adjust the EVAs' charging and vehicle-to-grid (V2G) operations to account for local voltage deviation, load variation and renewable generation variability in order to provide real-time adjustment mechanisms. By combining predictive analytics with control decision-making, the data-based control framework is intended to increase microgrid reliability, decrease the occurrence of voltage violations and increase the energy balance of a microgrid without negatively impacting EV drivers' mobility needs. Simulation results indicate that the data-based control framework is superior to traditional methods based on rule-setting due to improvements in voltage regulation performance, reductions in peak load demand and increased utilization of renewable energy resources than through the use of electric vehicles in intelligent microgrids.

Keywords: Electric vehicle aggregators, data-driven control, voltage regulation, vehicle-to-grid, multi-objective optimization.

1. Introduction

The transition from traditional power delivering systems to modern smart electricity grids is increasing as we see more integration of decentralized, digital, and distributed energy resources (RES). Smart microgrids offer a local method to manage RES, and they will help ensure that these RES can continue to meet our electrical needs reliably, efficiently, and resiliently. The challenge of having intermittent renewable generation sources (e.g., solar and wind) and variable loads can cause difficulties with maintaining energy balance and voltage regulation in smart microgrids. Of particular interest

Cite this article as: M. Kumar N, R.S.S. Nuvvula, and S. Gayathri D, "Data-Driven Control of Electric Vehicle Aggregators for Voltage and Energy Stability in Smart Microgrids," *Artificial Intelligence Research and Applications (AIra)*, Vol. 2, No. 3, pp. 149–155, September, 2026, https://doi.org/10.20508/ps000s93.

among flexible loads, are electric vehicles (EVs) because their growth rate is very high and they have large capacities for energy storage.

When EVs are grouped together and controlled in an intelligent manner, they can be used not only as loads on the electric grid, but also as distributed energy storage devices using their vehicle-to-grid (V2G) capability. Through the use of aggregators, EV owners can allow a third party to manage the charging and discharging of the EV batteries.

Aggregators are organizations that consolidate multiple EVs into an aggregated load and manage how they discharge into the electric grid. The ability to coordinate EV batteries with the electric grid enables the aggregation of multiple batteries to help maintain grid voltage and avoid negative impacts, such as transformer overloads, increased peak demand, etc. In addition, using aggregated EV batteries for grid services will help improve electrical grid performance and provide better ways to use electrical energy.

Static rules or pricing signals govern traditional electric vehicle (EV) charging methodologies, which do not readily adapt to the fast-changing conditions of the electrical grid. As microgrids become increasingly complex and data-rich, adaptive control approaches that utilize both real-time and historical data are needed. Data-driven control methodologies (machine learning, and advanced optimization techniques) are powerful methods to describe nonlinear system behaviour, forecast uncertainties and help make informed decisions.

This research is focused on creating a framework for data-driven control of electric vehicle aggregators to improve the voltage and energy stability in smart microgrids. Figure 1 illustrates the overall architecture of the proposed framework, in which predictive models are integrated with control algorithms to dynamically manage electric vehicle charging and discharging in response to grid conditions. The methodology maintains user constraints while coordinating flexible EV resources to support stable and efficient microgrid operation.

The remainder of this paper will include a literature review, provide a detailed description of the proposed methodology, an overview of implementation and experiment methods, and present the results and findings from this work, as well as provide suggestions for future work.

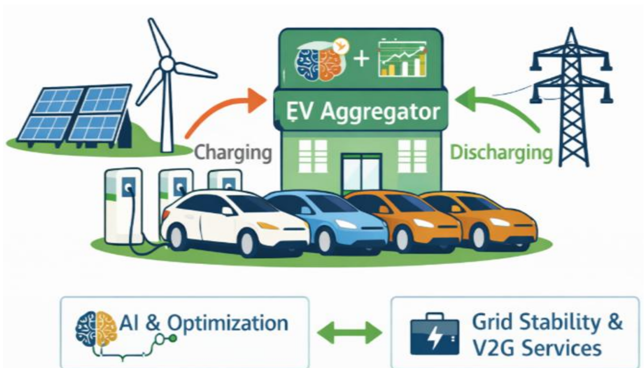

Fig. 1. Learning-driven coordinated EV energy management framework.

2. Literature Review

The involvement of electric vehicles in facilitating the operation of power systems has been investigated widely, particularly for using demand-response and distributed energy storage [1]. It has been shown that coordinated EV charging can help reduce peak demand and reduce the stress placed on distribution networks [2]. Uncoordinated EV charging, on the other hand, can lead to greater voltage deviations and increased losses, particularly within low-voltage microgrids with high penetration levels of renewable energy sources [3]. Therefore, there has been a lot of research done to develop control strategies that would allow EVs to directly assist in stabilising the grid [4].

EV aggregators have been introduced and leverage scalable concepts for managing very large amounts of EVs while meeting both grid requirements and user preferences [5].

Various centralised and decentralised control architectures have been proposed, including rule-based scheduling and optimisation-based energy management [6]. Optimisation-based approaches typically model the coordination of EV charging as a constrained optimisation problem with the aim of minimising costs, losses, or emissions while satisfying network and battery constraints [7]. While these approaches are generally very strong from an effectiveness perspective, many rely heavily on accurate system models and face challenges related to uncertainty and adaptability to changing conditions in real time [8].

To remedy the shortcomings listed above, many researchers have turned to data-driven and learning-based techniques [9]. Specifically, machine-learning models have been used to forecast EV charging demand [10], user behaviour [11], renewable generation [12], and load profiles [13]. These predictions may be used to control and schedule charging activities proactively and make better operational decisions [14].

Reinforcement learning has also been studied for real-time EV charging control, allowing agents to learn best practices through interaction with their environment [15]. Therefore, these learning-based techniques reduce dependency on explicit system models and improve the ability to adapt as operating conditions change [16].

Historically, voltage regulation within microgrids has been performed using reactive power controls, on-load tap changers, and energy storage systems [6]. The use of EVs within established voltage regulation methods provides additional flexibility; however, introducing EVs into voltage regulation schemes adds additional complexity.

Recent studies have investigated the use of EVs for voltage regulation through coordinated charging and discharging and concluded that coordinated charging improves voltage profiles and reduces violation rates, although most existing studies employ simplified scenarios or do not adequately assess performance under real-world uncertainties [16].

3. Methodology

The proposed learning-driven decision framework for coordinating electric vehicle (EV) energy exchange in renewable microgrids is implemented through the following sequential steps:

Step 1: Data acquisition and pre-processing: The EV aggregator constantly collects both historical data and real-time information from various sources, including renewal inverters, distribution-level sensors, EV telemetries, and charging stations. Collected data include measurements of bus voltage magnitude & angle; active/reactive power flow; arrival/departure timestamps; EV state-of charge. To prepare the data for later use, the following pre-processing methods will be utilized: removing missing values; filtering outliers; synchronizing different types of data streams; normalizing input values. Feature engineering will follow so as to create rich time-dependent (e.g., season, holidays...)/context based (e,g., temperature/lumens/ precipitation) indicators that will provide a solid foundations upon which predictive/control models can be constructed.

Step 2: Short-term forecasting and uncertainty modelling: Short-term forecasting for generating renewable energy, group demand from non-electricity vehicles, and the predictability of electric vehicle use is done using supervised learning models. These models utilize past data using cross-validation and are revisited to take into consideration seasonal deviations and changes in behaviour. Forecasts are generated not only as point estimates but also with associated uncertainty levels represented through quantiles or probabilistic scenarios using techniques such as ensemble learning or quantile regression, thereby accounting for inherent variability and ensuring improved robustness against forecast uncertainty under uncertain operating conditions, as illustrated in Fig. 2.

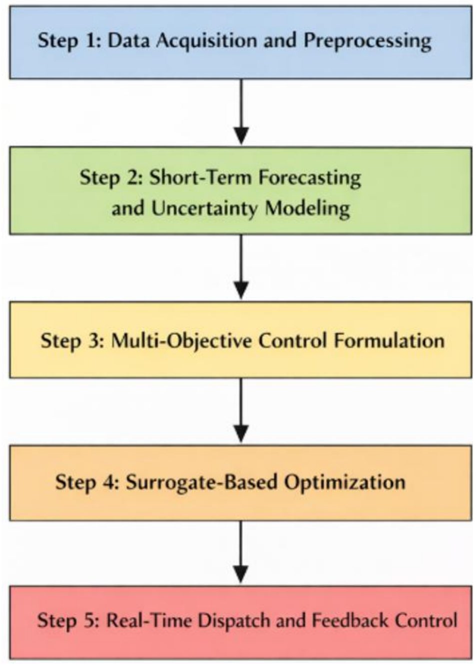

Fig. 2. Data-driven EV aggregator control scheme for voltage and energy stability.

Step 3: Multi-objective control problem formulation: In every control interval a formulation is provided for the solution of a multi-objective optimization problem. Objectives will include minimizing voltage deviations at critical load buses, reducing maximum net load (peak net load), and maximizing local renewable energy utilisation (utilisation of renewable energy generated locally). Constraints defined in the system pertain to network power flow limits, transformer capacity limits, EV battery charging and discharging limits, and minimum state of charge required to depart based on user mobility requirements. A composite weighted objective function is developed to determine trade-offs among the competing objectives of each control interval; the weights are selected based on operator preference, utilizing a sensitivity analysis.

Step 4: Surrogate-based optimization and decision making: To solve nonlinear AC power flow issues, an EV charging and discharging surrogate system (or mapping) for power flow analysis will be created based on historical or simulated data to quickly assess the performance of any EV charging (or discharging) control strategy without having to conduct a complete analysis of the system. Once the surrogate is completed, a constrained numerical optimization solution using warm-start to solve will be applied. Forecasting methods will be used as well as scenario generation/analysis and chance constraint methods, all to increase future robustness to forecast errors.

Step 5: Real-time dispatch and closed-loop feedback: As shown in Table 1, aggregators send optimized EV charging and V2G setpoints to individual EVs while respecting user-defined flexibility windows. The microgrid continuously monitors real-time feedback and detects deviations arising from unexpected EV behaviour or communication delays. Performance threshold violations trigger re-optimization to limit excessive cycling and associated battery degradation costs, while incentive-compatible mechanisms are employed to ensure user compliance. Hierarchical control structures support scalability for large EV fleets, and event-triggered updates with local fallback policies ensure safe operation under degraded communication conditions.

4. Implementation and Experimental Setup

A low-voltage smart microgrid was simulated in a time series to evaluate the implementation. Distributed photovoltaic generation, residential and commercial loads, and centralized aggregation of EVs comprise this microgrid. The network topology includes many radial feeders and monitored buses selected as representative sites of where voltage sensitivity may exist. Datasets were used to create PV profiles and load tracing that reflect anticipated levels of high renewable penetration and peak when exercising.

Heterogeneous battery sizes, charging limitations, and user schedules are used to simulate an EV fleet that reflects real-world variability in charging behaviour. Several probabilistic patterns were used to create multiple arrival/delivery scenarios for all vehicles in the e-fleet.

Table 1. Comparative analysis of EV charging, V2G control, and energy management approaches

Ref.	Focus Area	Method / Approach	Key Findings
[1]	Vehicle-to-Grid (V2G) integration	Mathematical modeling and MATLAB/Simulink simulation	Demonstrated effective bidirectional power flow between EVs and grid; V2G improves grid support and peak load management
[2]	Bidirectional on-board charger for EVs	Soft-switching Dual Active Bridge (DAB) converter with optimized control	Achieved high efficiency and reduced switching losses during V2G and G2V operation
[3]	Bidirectional DC–DC converter for EVs	Design and experimental validation of converter topology	Validated reliable V2G/G2V operation with improved power quality and efficiency
[4]	EV aggregation for frequency control	Optimal coordinated control strategy in microgrids	EV aggregation significantly enhances frequency stability under varying operating conditions
[5]	Fast charging power converters	Comparative analysis of converter topologies and control methods	Identified suitable converter configurations for ultra-fast EV charging with high power density
[6]	EV charging station communication	Heterogeneous communication network with multi-aggregator architecture	Improved charging station coordination under high PV variability using distributed sensors
[7]	EV aggregator scheduling	Optimization-based scheduling for frequency regulation	Reduced operational costs while improving frequency regulation in renewable-powered grids
[8]	DC microgrid voltage stability	GaN-based bidirectional converter with fuzzy logic controller	Enhanced voltage stability and dynamic response during EV charging
[9]	EV charging communication networks	Heterogeneous communication network with multi-aggregator architecture	Improved charging station coordination under high PV variability using distributed sensors
[10]	Energy management for xEV charging stations	Adaptive energy management strategy in hybrid microgrid	Improved sustainability, reduced grid dependency, and optimized energy usage
[11]	Smart EV charging networks	AI-based demand response integrated with blockchain	Enhanced load balancing, transparency, and security in EV charging operations
[12]	Renewable energy site selection	Multi-Criteria Decision Making (MCDM) approach	Provided optimal wind power location selection considering technical and economic factors
[13]	Load frequency control	Integration of EVs and energy storage systems	Combined EVs and ESS improved frequency regulation in isolated microgrids

Chargers will allow for bi-directional power flow (V2G) when V2G is allowable. Battery models will account for SOC/dynamics and provide a simple degradation estimate (by energy throughput). Hard constraints on the minimum SOC of the EV upon departing from the charger (to meet user mobility needs) and soft penalties for delaying charging or having to accommodate any user preference-based inconvenience will be imposed.

An integrated simulation system of a control layer implementing a data-driven aggregator and a power flow engine to evaluate AC networks. The simulation framework was implemented in Python, utilizing scikit-learn for supervised learning models, NumPy and Pandas for data preprocessing, and a standard AC power flow solver for network evaluation.

Surrogate models were developed and validated using historical operational data. Models will be developed from historical sequences (offline) and then updated on a regular schedule, providing updated rolling forecasts, including the confidence level for each prediction. The multi-objective optimizer generates aggregate charging set-points to individual vehicles at regular intervals. Communications assessment includes realistic latencies and packet loss to evaluate resiliency. The baseline of the simulations will use a basic rule-based strategy for determining when to begin charging a vehicle (on arrival) or to delay charging until off-peak times with no coordinated V2G support.

5. Results and Discussion

The simulation results show a data-driven aggregator improving voltage regulation, peak demand, and renewable use through a coordinated control system compared to a baseline rule-based approach. As shown in Figure 3, the time series of voltage magnitudes across monitored buses shows how much less often voltages excursion from nominal voltage values are occurring and how many fewer times below threshold violations occurred with coordinated control compared to rule-based control.

In addition, strategic shifts in charging to times when there are more renewable energy available and managed discharges during daylight peak demand periods will produce a reduction in the peak net load. Figure 4 demonstrates the continued smoothing of feeder demand as a result of these changes, which will serve to reduce maximum loading and thermal loading of transformers and conductors.

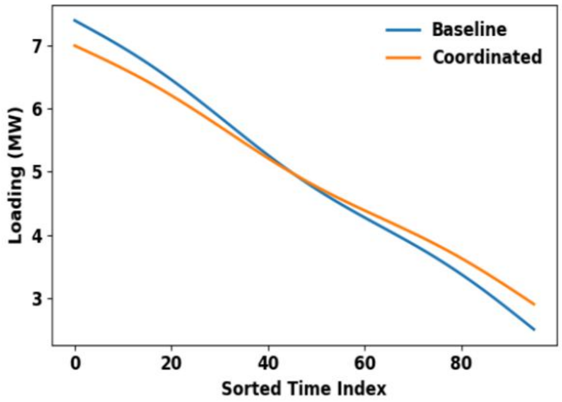

Fig. 3. Feeder load duration curve under baseline and coordinated control.

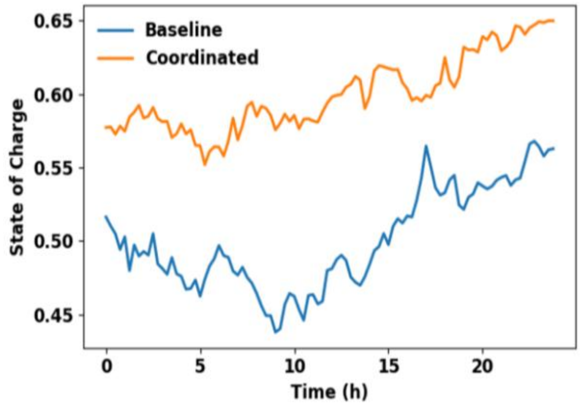

Fig. 4. Impact of coordinated aggregation on EV state-of-charge profiles.

At the same time, as more energy generated by the fleet can be consumed through the addition of stored energy in vehicles during periods of excess generation, the amount of curtailment experienced by PV systems can be reduced. In Figure 5, the various simulations show clear improvements in peak net demand and total renewable energy curtailment when using the coordinated method compared to the baseline methods. These improvements are observed across different operating conditions, demonstrating the effectiveness and robustness of the proposed coordinated control strategy. The quantitative performance improvements for each scenario are summarized in Table 2, further highlighting the reductions in peak demand and renewable energy curtailment achieved by the coordinated approach. The system's forecasting capabilities also support decision-making earlier than traditionally possible, as can be seen in Figure 6. The ability to forecast accurately in the short-term allows an aggregator to position the charge schedule ahead of time to prevent future voltage violations from occurring, and if forecast errors increase above a certain amount, the closed-loop system will perform re-optimizations to correct the error(s).

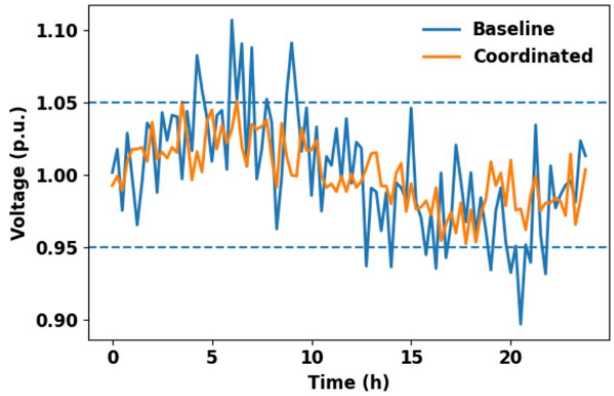

Fig. 5. Voltage magnitude at a representative bus under baseline and coordinated control.

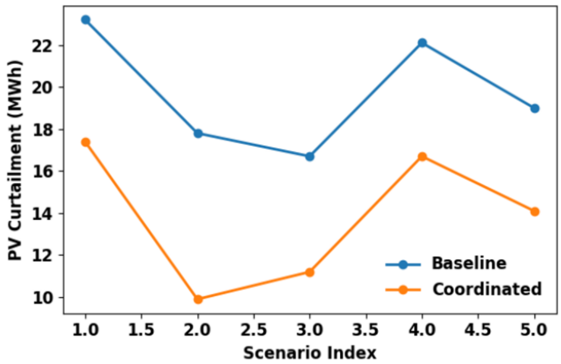

Fig. 6. Comparison of PV curtailment under baseline and coordinated strategies.

Table 2 : Performance comparison of baseline rule-based control and coordinated aggregator control.

Metric	Baseline (Rule-Based)	Coordinated (Data-Driven)	Observed Improvement
Voltage excursions from nominal	Frequent excursions and violations	Significantly reduced excursions	Improved voltage regulation
Below-threshold voltage violations	Multiple occurrences	Rare to none	Enhanced feeder reliability
Peak net feeder load	Higher peak demand	Reduced and flattened peaks	Lower transformer/conductor loading
Feeder load profile	Sharp peaks, less smooth	Smoothed demand profile	Reduced thermal stress
Renewable energy curtailment	Higher PV curtailment	Lower curtailment	Increased renewable utilization
EV state-of-charge alignment	Poor alignment with PV output	Charging aligned with high PV availability	Better energy absorption
Sensitivity to forecast error	No anticipatory control	Graceful degradation with uncertainty	Improved robustness

6. Conclusion

The research introduced a data-driven control system that provides EV aggregators a way to assist with voltage and overall energy stability of smart microgrids. As a means of accomplishing this, real-time telemetry was integrated with short-term forecasts, surrogate voltage models and multi-objective optimization so that the aggregator could efficiently coordinate charging of EVs and V2G operations, reducing voltage violations, smoothing the net load, and increasing the use of local renewables. In addition, the combination of constraints and penalty terms in this approach maintained the mobility needs of users while also limiting degradation of batteries, thus allowing this service to be provided in a manner that does not compromise on the expectations of EV owners.

Simulation-based evaluations using representative microgrid scenarios showed significant improvements over a rule-based baseline, including reduced voltage excursions, decreased peak net load, lower renewable energy curtailment, and improved robustness under forecast uncertainty and communication interruptions. Sensitivity analyses revealed that the closed-loop adaptive control method will maintain its robustness when faced with moderate forecast error and communication interruptions; however, performance will suffer significantly when there is little to no data available or when there are long periods of time with no connectivity. The use of surrogate models for computing has resulted in the ability to operate in near real-time for the scale of the studied system.

Author Contributions

All authors contributed to conceptualization, methodology, software, data curation, formal analysis, investigation, visualization, writing-original draft, writing-review, editing and have read and approved the final version of the manuscript.

Acknowledgements

Not applicable.

Conflict of Interest

The authors declare no conflict of interest.

References

[1] G. Janardhan, R. Shanmugasundaram, S. K. J., R. Narendar, and S. K. K., “Modeling and simulation of vehicle to grid (V2G) integration,” *E3S Web of Conferences*, vol. 616, p. 01016, 2025, doi: 10.1051/e3sconf/202561601016.

[2] V. Sonnati, S. Arandhakar, and K. S. V. P. Kumar, “Soft-switching dual active bridge converter-based bidirectional on-board charger for electric vehicles under vehicle-to-grid and grid-to-vehicle control optimization,” *E3S Web of Conferences*, vol. 472, p. 01021, 2024, doi: 10.1051/e3sconf/202447201021.

[3] Y. Meadari, D. Harsha, P. K. Biswas, and T. S. Babu, “Design and development of bidirectional converter based on V2G and G2V operation,” *E3S Web of Conferences*, vol. 547, p. 03002, 2024, doi: 10.1051/e3sconf/202454703002.

[4] S. Iqbal, S. Habib, N. H. Khan, M. Ali, M. Aurangzeb, and E. M. Ahmed, “Electric vehicles aggregation for frequency control of microgrid under various operation conditions using an optimal coordinated strategy,” *Sustainability*, vol. 14, no. 5, p. 3108, 2022, doi: 10.3390/su14053108.

[5] V. Manoj, R. Pilla, and S. R. Sura, “A comprehensive analysis of power converter topologies and control methods for extremely fast charging of electric vehicles,” *Journal of Physics: Conference Series*, vol. 2570, no. 1, p. 012017, 2023, doi: 10.1088/1742-6596/2570/1/012017.

[6] M. Davila-Sacoto, L. Hernández-Callejo, L. G. González, Ó. Duque-Perez, Á. L. Zorita-Lamadrid, and D. Ochoa-Correa, “Heterogeneous communication network architecture for the management of electric vehicle charging stations: multi-aggregator management in microgrids with high photovoltaic variability based on multiple solar radiation sensors,” *Sensors*, vol. 24, no. 12, p. 3768, 2024, doi: 10.3390/s24123768.

[7] S. Ma, “Optimal scheduling of electric vehicle aggregators for frequency regulation and cost efficiency in renewable-powered grids,” *Computers & Electrical Engineering*, vol. 118, p. 109317, 2024, doi: 10.1016/j.compeleceng.2024.109317.

[8] K. Padma and K. Manohar, “Voltage stability in a photovoltaic-based DC microgrid with GaN-based bidirectional converter using fuzzy controller for EV charging applications,” *WSEAS Transactions on Systems and Control*, vol. 19, pp. 143–152, 2024, doi: 10.37394/23203.2024.19.15.

[9] S. Tabassum, A. R. V. Babu, and D. K. Dheer, “Adaptive energy management strategy for sustainable xEV charging stations in hybrid microgrid architecture,” *Science and Technology for Energy Transition*, vol. 80, p. 22, 2025, doi: 10.2516/stet/2025002.

[10] A. R. Singh, R. S. Kumar, K. R. Madhavi, F. Alsaif, M. Bajaj, and I. Zaitsev, “Optimizing demand response and load balancing in smart EV charging networks using AI integrated blockchain framework,” *Scientific Reports*, vol. 14, no. 1, p. 31768, 2024, doi: 10.1038/s41598-024-82257-2.

[11] V. Manoj, V. Sravani, and A. Swathi, “A multi-criteria decision-making approach for the selection of optimum location for wind power project in India,” *EAI Endorsed Transactions on Energy Web*, p. 165996, 2018, doi: 10.4108/eai.1-7-2020.165996.

[12] R. R. Shukla, M. M. Garg, and A. K. Panda, "Driving grid stability: Integrating electric vehicles and energy storage devices for efficient load frequency control in isolated hybrid microgrids," *Journal of Energy Storage*, vol. 89, p. 111654, 2024, doi: 10.1016/j.est.2024.111654.

[13] A. Rajagopalan, K. Nagarajan, M. Bajaj, S. Uthayakumar, L. Prokop, and V. Blazek, "Multi-objective energy management in a renewable and EV-integrated microgrid using an iterative map-based self-adaptive crystal structure algorithm," *Scientific Reports*, vol. 14, no. 1, p. 15652, 2024, doi: 10.1038/s41598-024-66644-3.

[14] R. Battula and S. Vuddanti, "Distributed control strategy for secondary frequency regulation with EV demand aggregation and delay compensation in AC unbalanced microgrid," *Electric Power Systems Research*, vol. 225, p. 109782, 2023, doi: 10.1016/j.epsr.2023.109782.

[15] H. R. Sayarshad, "Designing vehicle-to-grid (V2G) aggregator fleet capacity for power grid reliability against cyberattacks," *Electric Power Systems Research*, vol. 244, p. 111554, 2025, doi: 10.1016/j.epsr.2025.111554.

[16] M. B. Prasad, P. Ganesh, K. V. Kumar, P. A. Mohanarao, A. Swathi, and V. Manoj, "Renewable energy integration in modern power systems: Challenges and opportunities," *E3S Web of Conferences*, vol. 591, p. 03002, 2024, doi: 10.1051/e3sconf/202459103002.

Artificial Intelligence Research and Applications (AIra)
https://www.ijaira.org/ Online ISSN: 3108-3889
K.N. Khallouf and H. Benbouhenni, Vol. 2, No. 3, September, 2026 Research Article

Fuzzy Logic–Based Control for Photovoltaic Systems with Integrated Energy Storage

Khaoula Nermine Khallouf*, Habib Benbouhenni**‡

* Department of Electrical Engineering, Laboratory of mod ERNA, Mentouri Univ. of Constantine 1, Constantine, Algeria.

** Department of Electrical Engineering, Faculty of Technology, Hassiba Benbouali University of Chlef, B.P 78C Ouled Fares, Chlef 02180, Algeria.

(khaoula-nermine.khallouf@student.umc.edu.dz, h.benbouhenni@univ-chlef.dz)

‡ Corresponding Author: Habib Benbouhenni, Hassiba Benbouali University of Chlef, h.benbouhenni@univ-chlef.dz.

Received: 08.11.2025, Revised: 12.04.2026, Accepted: 05.05.2026

Abstract- The application of fuzzy logic control (FLC) to a photovoltaic (PV) system with an energy storage solution aims to enhance the efficiency, reliability, and stability of renewable energy generation. In such systems, solar panels convert sunlight into electrical power, while a storage device—typically a battery—stores excess energy for later use or grid support. Because PV output fluctuates due to changing weather conditions and varying solar irradiance, maintaining optimal energy flow and battery management becomes complex. FLC method provides an effective solution by mimicking human decision-making through a set of linguistic rules rather than relying on precise mathematical models. This allows the controller to handle the nonlinear and uncertain behaviour of PV systems. The FLC technique can dynamically regulate parameters such as the duty cycle of DC–DC converters, battery charge/discharge rates, and power balance between the PV array, the battery, and the load or grid. Compared with conventional control methods (e.g., PID control), FLC method offers better adaptability and robustness under rapidly changing environmental conditions. Simulation and experimental results reported in research show that FLC approach improves system performance by achieving smoother power output, faster response to irradiance variations, and prolonged battery lifespan through optimized energy management. In summary, integrating FLC method into PV systems with storage enhances energy conversion efficiency, system stability, and overall reliability—making it a valuable method for modern smart grids and sustainable energy applications.

Keywords: Fuzzy logic, photovoltaic system, DC–DC converters, renewable energy generation, energy storage.

1. Introduction

Fuzzy logic (FL), first introduced by Lotfi A. Zadeh in 1965, is an extension of classical Boolean logic, designed to handle approximate rather than fixed and precise reasoning [1]. Unlike traditional binary logic, where variables must take values of either 0 or 1, FL method allows variables to have truth values ranging from 0 to 1. This capability makes it particularly suitable for systems involving uncertainty, inaccuracy, or complex nonlinear relationships, which are common characteristics in renewable energy systems [2].

In renewable energy applications, FL controllers (FLCs) are increasingly used in decision-making, control, and optimization tasks, due to their ability to mimic human reasoning and adapt to changing environmental conditions [3]. For example, FLC method has been used in maximum power point tracking (MPPT) for photovoltaic (PV) power systems [4], wind turbine control [5], energy management in hybrid renewable energy systems [6], and load forecasting [7].

Cite this article as: K.N. Khallouf and H. Benbouhenni, “Fuzzy Logic–Based Control for Photovoltaic Systems with Integrated Energy Storage,” *Artificial Intelligence Research and Applications (AIra)*, Vol. 2, No. 3, pp. 156–166, September, 2026, https://doi.org/10.20508/qtrxhx79.

Each of these applications offers distinct advantages. FLCs do not require a precise mathematical model of the system, making them robust to parameter variations and measurement noise [8]. They can also efficiently handle nonlinear interference in wind and solar power conversion processes and adapt to rapidly changing weather conditions. Furthermore, fuzzy systems are relatively easy to integrate with other control algorithms, such as neural networks or genetic algorithms [9, 10], forming powerful hybrid intelligent controllers.

However, there are also drawbacks. Designing an effective FL system often relies on expert knowledge to define membership functions and rules, which can be subjective and time-consuming [11]. FL systems may require extensive tuning for varying operating conditions, and their performance may deteriorate when applied to systems beyond the scope of the initial design. In addition, compared to model-based control methods, FL may sometimes lack transparency and interpretability, especially in large-scale applications [12]. In general, FL provides a flexible and effective framework for managing uncertainty and improving the performance of renewable energy systems [13]. Its adaptability and robustness make it a valuable tool for optimizing energy generation and consumption, although careful design and validation are essential to overcome its inherent limitations [14].

Combining FL method with advanced control strategies, such as direct power control (DPC) [15], space vector control (or space vector)/switch table control (STC) [16], field-oriented control (FOC) [17], slide mode control (SMC) [18], and backstepping control (BC) [19], enhances the overall robustness, adaptability, and dynamic performance of electric motor and power converter systems. FL method can be incorporated as an intelligent supervisor or adaptive tuner that adjusts control gains, switching thresholds, or reference parameters in real time, compensating for modeling uncertainty, nonlinearity, and external disturbances. In DPC method and self-tuning control (STC) systems, fuzzy rule sets facilitate switching and reduce torque and flux ripples. When applied with a FOC system, fuzzy inference improves the accuracy of speed and current loops under varying load conditions. In SMC and BC techniques, FL method can mitigate the effects of oscillation and simplify the design of control laws by replacing complex mathematical models with rule-based approximations. Overall, the hybridization of FL method with these nonlinear control techniques achieves a more flexible and error-resistant control architecture, suitable for high-performance electric drives and renewable energy systems.

Photovoltaic (PV) systems, which convert sunlight directly into electricity using semiconductor materials, have become one of the most promising and fastest-growing renewable energy technologies in the modern world [20]. Their importance in the energy and industrial sectors stems from the global need to reduce dependence on fossil fuels, lower greenhouse gas emissions, and promote sustainable energy solutions [21]. PV power systems offer many advantages, including clean and quiet operation, low maintenance and installation requirements, and the ability to deploy in diverse environments-from rooftops and remote rural areas to large-scale solar farms and industrial facilities [22]. Furthermore, advances in PV materials, power electronics, and energy storage have improved their efficiency and integration into smart grids and hybrid energy systems. However, despite their advantages, PV power systems face several drawbacks and challenges [23]. Their energy production is inherently intermittent and weather-dependent, leading to fluctuations in power output and necessitating reliable energy storage or backup systems. While initial installation costs may decrease over time, they remain relatively high compared to conventional energy sources, particularly in developing regions [24]. In addition, issues related to energy conversion efficiency, land use for large installations, and the environmental impact of PV panel manufacturing and disposal must be addressed. In the industrial and commercial sectors, PV systems are widely used to power manufacturing plants, telecommunications, agricultural irrigation, and remote monitoring systems [24]. Key challenges hindering widespread adoption include limited energy storage technologies, grid integration difficulties, and the need for supportive policies and infrastructure. Overcoming these obstacles will be essential to realizing the full potential of PV systems as a cornerstone of a sustainable and resilient energy future [25].

This work addresses the enhancement of performance, stability, and energy efficiency in PV power conversion and management by proposing an intelligent control strategy based on a FLC method. The main contribution of this study is the design, implementation, and comprehensive simulation of an FLC capable of effectively regulating power flow between the PV array, the energy storage system, and the load under varying operating conditions such as changes in irradiance, temperature, and load demand. In addition, a systematic comparative analysis with a conventional PI controller is conducted to highlight the advantages of the proposed approach. This comparison focuses on key performance indicators, including reference tracking accuracy, reduction of current and power ripples, minimization of response time, overshoot and undershoot in DC-link voltage, and mitigation of THD in the current. The results demonstrate that the proposed FLC provides superior robustness, adaptability, and dynamic performance, particularly in handling the nonlinearities and uncertainties inherent in PV systems. Overall, the study confirms the effectiveness of the proposed control strategy in improving system efficiency, reducing energy losses, and enhancing the reliability of hybrid PV systems with energy storage.

The main objectives achieved in this work are summarized as follows:

- Maintaining the stability of the DC-link voltage under varying operating conditions.
- Improving the charging and discharging performance of the energy storage unit.
- Ensuring continuous and reliable power supply despite fluctuations in irradiance and load.
- Reducing current and power ripples and minimizing harmonic distortion.
- Enhancing dynamic response by reducing rise time, overshoots, and undershoots.

- Increasing overall energy efficiency and reducing system losses.
- Demonstrating the superiority of the FLC approach over the conventional PI controller.

The manuscript has five distinct sections. Following the introduction, the modelling and design of the microgrid system proposed in this paper are presented. Section three details the control approach applied to the microgrid system, highlighting its key advantages over traditional methods. Section four presents the results obtained from both the traditional and the designed approaches, including numerical data. In the fifth section, the most important conclusions obtained from this work are listed, along with a proposal for future work as a complement to this work

2. Design and Modelling of the Microgrid (MG) System

This paper is devoted to the study of the MG system associated to the PV system. The form of the designed structure is presented in Figure 1. Relying on this system allows for a reduction in the use of non-renewable resources, thus mitigating the effects of global warming. Furthermore, its use reduces the costs of energy production and consumption. This system can be installed on rooftops, creating several practical solutions that significantly contribute to the development of the electrical energy sector. This system, designed in this study, is highly effective in isolated and remote areas, as its adoption greatly reduces power transmission lines and the damage these lines cause to arable land.

This structure involves the connection of all converter systems via a common DC bus. The inspected system consists of a PV energy system, and a battery energy storage system (ESS). The PV system consists of a PV array associated with the DC-DC-BC, and the battery-ESS is composed of the BS and the DC/DC reversible chopper. All these converter systems are linked through a common DC bus to the coupling point (PCC) by the Multifunctional voltage source inverter (MFVSI), feeding a nonlinear load.

To extract the ME conversion from the system, a comparative work between two types of control, traditional PI and intelligent artificial FLC, the maximum power point tracking (MPPT) based on PI control and the FLC technique were applied in the control at each converter in the system, and at the MFVSI inverter to get better the power quality at the PCC.

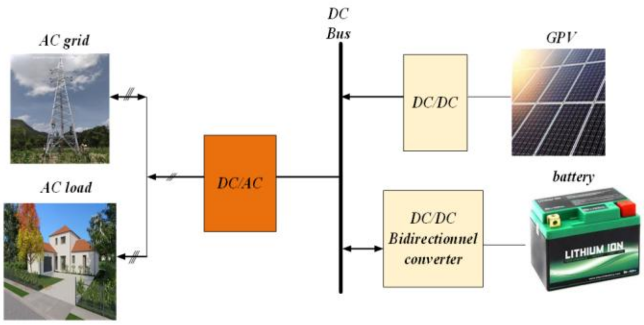

Fig. 1. The designed power system.

2.1. PV System Model

A solar cell is a device that converts solar energy into electricity using the PV effect, which is closely related to the P-N junction of semiconductors. In this study, a PV cell model based on the static behaviour of a conventional P-N junction diode is used [26]. The electrical model includes a current source in parallel with a diode, a shunt resistance (r_{sh}), and a series resistance (r_s). The shunt resistance represents current leakage and parasitic currents due to material defects or impurities, while the series resistance accounts for the internal resistance of the semiconductor and its connections. It is important to arrange the modules in series, parallel, or a mixed configuration to form a PV array capable of delivering appropriate voltage and power levels, potentially reaching several kilowatts. The equivalent circuit is shown in Figure 2 [23].

The output current of the PV array is mathematically expressed as [21]:

$$i_{pv} = N_p I_{ph} - N_p I_0 \cdot \left[exp\left(\frac{q}{N_s N_p \gamma KT}\left(V_{pv} + \frac{N_s}{N_p} r_s i_{pv}\right)\right) - 1\right] - \frac{\left(v_{pv} + \frac{N_s}{N_p} r_s i_{pv}\right)}{\frac{N_s}{N_p} r_{sh}} \quad (1)$$

2.2. Modelling of the DC-DC Converter in the PV System

The DC-DC boost converter is designed to increase the voltage supplied by the PV array to an optimal level, thereby maximizing energy production [27]. A capacitor is typically placed between the generator and the boost converter to reduce high-frequency harmonics. Figure 3 shows a schematic diagram of the DC-DC boost converter used in the system under study. This type was chosen for its simplicity and ease of implementation. Furthermore, this converter is easy to control, making it a superior choice.

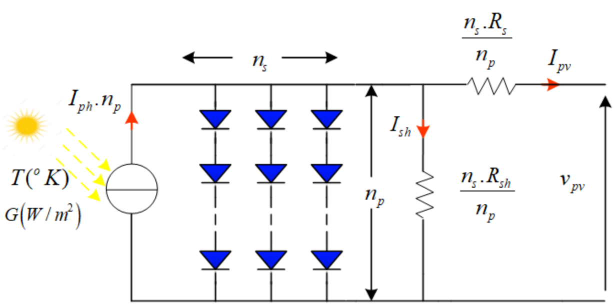

Fig. 2. Equivalent circuit of the PV array.

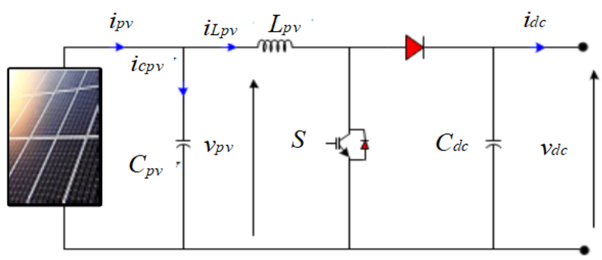

Fig. 3. Equivalent circuit of the PV array.

The differential equations governing the dynamics of the input voltage and the current through the inductor are expressed as follows [28]:

$$\begin{cases} C_{pv}\dfrac{dv_{pv}}{dt} = i_{pv} - i_L \\ \dfrac{di_L}{dt} = \dfrac{1}{L_{pv}} v_{pv} - (1-D)\dfrac{1}{L_{pv}} v_{dc} \end{cases} \tag{2}$$

Here, v_{pv} and i_{pv} represent the voltage and current generated by the PV array, respectively, while i_L denotes the current flowing through the inductor of the DC-DC converter. v_{dc} refers to the DC bus voltage, D is the duty cycle, and C_{PV} and L_{PV} are the electrical parameters of the boost converter

2.3. Mathematical Models of Batteries

Although Li-ion batteries are relatively expensive, they offer outstanding performance due to their high energy density, output voltage, and low self-discharge rate, making them especially suitable for microgrids [29]. This is illustrated by the Berger model, shown in the Figure 4.

The mathematical model of the battery in charge/discharge mode is given in [30]:

- Charging mode:

$$\begin{aligned} V_{dis} &= E_0 - K\frac{Q}{Q-it}(i_t) - R_{int}i + A.e^{-B\times t} - K\frac{Q}{Q-it}i^* \\ &= E_0 - \underbrace{R_{int}i}_{V_{ohm}} - \underbrace{K\frac{Q}{Q-it}\left(i_t + i^*\right)}_{V_{pol}} + V_{exp} \end{aligned} \tag{3}$$

- Discharging mode:

$$\begin{aligned} V_{ch} &= E_0 - K\frac{Q}{Q-it}(i_t) - R_{int}i + A.e^{-B\times t} - K\frac{Q}{it-0.1Q}i^* \\ &= E_0 - \underbrace{R_{int}i}_{V_{ohm}} - \underbrace{K\frac{Q}{Q-it}\left(\frac{Q}{Q-it}i_t + K\frac{Q}{it-0.1Q}i^*\right)}_{V_{pol}} + V_{exp} \end{aligned} \tag{4}$$

The battery output voltage (V_b) is defined by the discharge voltage (V_{dis}) and the charge voltage (V_{ch}). (E_0) represents the reference voltage during charging. The maximum battery capacity is denoted by Q (Ah), and it includes a polarization constant K (V/Ah), internal resistance R_{int} (Ω), and discharge current i_b (A).

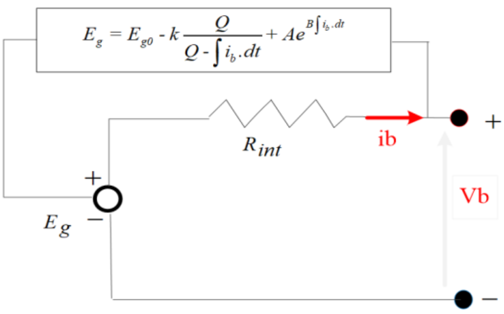

Fig. 4. Equivalent model of a battery.

The instantaneous discharge current is represented by ($i_b \times t$), and the filtered discharge current is noted as i_b^* (A). Finally, A refers to the amplitude of the exponential zone (V), and B is the inverse time constant for this exponential zone (Ah^{-1}).

The state of charge (SOC) of a battery can be estimated based on the discharge current and the battery capacity:

$$SOC = SOC_0 - \frac{1}{Q}\int idt \tag{5}$$

2.4. Mathematical Model of the Bidirectional DC-DC Converter in the Storage System

For energy conversion in a battery ESS, a bidirectional flow of electrical energy is required. To achieve this, a bidirectional DC-DC current converter has been integrated into the control system [31]. The corresponding schematic of the converter is shown in Figure 5.

The following equations describe the dynamic model of the BESS (Battery Energy Storage System).

$$\begin{cases} \dfrac{di_b}{dt} = \dfrac{V_b - i_b R_b - D_b.v_{dc}}{L_b} \\ \dfrac{dv_{dc}}{dt} = \dfrac{1}{C_{dc}}\left(V_b - i_b D_b - i_{dc}\right) \end{cases} \tag{6}$$

2.5. Mathematical Model of the AC Side

Figure 6 shows the equivalent electrical diagram of the AC side, which includes a MFVSI, a nonlinear load, and an AC grid.

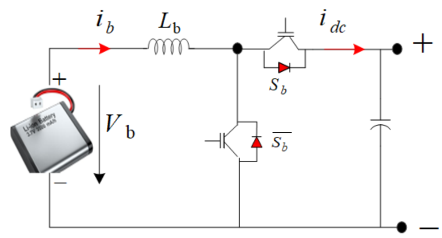

Fig. 5. Topologies of the bidirectional converter.

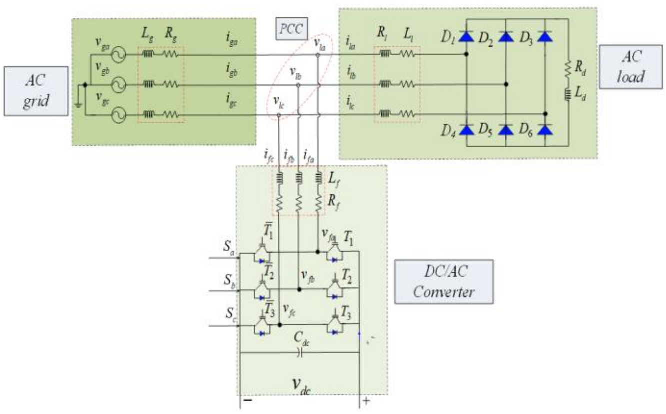

Fig. 6. Equivalent electrical diagram of the AC side.

The equation linking the grid-side current and voltage is derived using Kirchhoff's laws applied to the above circuit and can be expressed as follows:

$$\frac{di_{gabc}}{dt} = \frac{1}{L_f} v_{gabc} - \frac{R_g}{L_g} i_{gabc} + \frac{1}{L_g} v_{\ell_{abc}} \tag{7}$$

The load consists of a three-phase diode rectifier (Graetz bridge), connected to the grid through a line impedance (Z), supplying an inductive load (R and L), as shown in Figure 6. The inductance (L) varies between 1–10% of its nominal value and is expressed as:

$$L_\ell = \frac{v_g}{\omega . i_{\ell a}} \tag{8}$$

with:

$$i_{\ell a} = \sqrt{\frac{3}{2}} i_d \tag{9}$$

The behaviour of the APF currents in a three-phase reference frame is described by the following system of equations [32]:

$$\begin{cases} \dfrac{di_{f_{abc}}}{dt} = -\dfrac{R_f}{L_f} i_{fabc} + \dfrac{1}{L_f} v_{f_{abc}} - \dfrac{1}{L_f} v_{\ell abc} \\ \dfrac{dv_{dc}}{dt} = \dfrac{1}{C_{dc}} i_{dc} - S_{abc} i_{fabc} \end{cases} \tag{10}$$

The expressions of the inverter's phase (line-to-neutral) voltages based on the switching states (S_a, S_b, S_c) are given by the following equation:

$$\begin{cases} v_{f1} = \dfrac{V_{dc}}{3}(2S_a - S_b - S_c) \\ v_{f2} = \dfrac{V_{dc}}{3}(2S_a - S_b - S_c) \\ v_{f3} = \dfrac{V_{dc}}{3}(2S_c - S_b - S_a) \end{cases} \tag{11}$$

3. The Proposed Control Method of Converter of the MG

FL operators are mathematical functions defined on the interval [0, 1] that allow the combination of degrees of truth. They extend the classical Boolean operators "AND", "OR", and "NOT".

The intersection of two fuzzy sets A and B is defined as:

$$\mu_{A \cap B}(x) = min\left(\mu_A(x), \mu_B(x)\right) \tag{12}$$

The union of two fuzzy sets A and B is defined as:

$$\mu_{A \cup B}(x) = max\left(\mu_A(x), \mu_B(x)\right) \tag{13}$$

The complement of a fuzzy set is characterized by the following membership function:

$$\mu_{\bar{A}}(x) = 1 - \mu_A(x) \tag{14}$$

The fuzzy controller features a modular architecture consisting of three main blocks, as illustrated in Figure 7. These modules are: fuzzification, inference module, and defuzzification.

According to Figure 7, the FLC system consists of the following key components:

- Acquisition: Measurement of the output using an analog/digital sensor.
- Processing: Calculation of the error (e) and its variation (Δe), followed by normalization using the gains Ke, KΔe, and KΔu.
- Fuzzy Core: Includes the FL rule base and the defuzzification process (conversion to a numerical control value).
- Control Generation: Integration of Δu (summation) and application of the final control law.

The form of the control law is given by:

$$u\,(k+1) = u_k\,(k) + K_{\Delta u}.\Delta u(k) \tag{15}$$

Where *KΔu* and *Δu(k)* represent the gain associated with the control signal *u(k+1)* and the variation in the control action, respectively.

The error (e) and its variation (Δe) are defined as follows:

$$\begin{cases} E_e = K_e.e \\ E_{\Delta e} = K_{\Delta e}.\Delta e \end{cases} \tag{16}$$

Where, *Ke* and *KΔe* are the normalization factors, which play a critical role in the performance of the control system.

The membership functions were designed using a heuristic approach based on the system dynamics and control objectives. Specifically, symmetrical triangular and trapezoidal membership functions were adopted due to their simplicity and effectiveness, ensuring full coverage of the input (error and change of error) and output domains. The ranges of these functions were selected according to the expected operating limits of the system and have now been explicitly illustrated in the manuscript.

The proposed FLC employs a total of 49 fuzzy rules (7×7), constructed based on expert knowledge and the desired control behavior linking the error and its variation to the control action. These rules are now clearly presented in the form of a rule table for improved clarity and reproducibility.

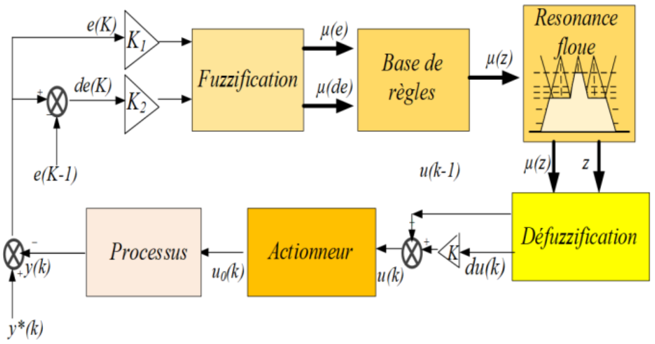

Fig. 7. Structure of the FLC.

Regarding the normalization gains (Ke, KΔe, KΔu), they were initially selected based on the system's operating range to properly scale the input and output variables into normalized fuzzy domains.

Subsequently, these gains were fine-tuned through an iterative trial-and-error procedure using simulation results, with the objective of achieving optimal performance in terms of fast response, minimal overshoot, and reduced steady-state error (SSE). The final selected values are now reported in the revised manuscript.

Figure 8 represents the membership functions used in this work to embody the mysterious controller.

Table 1 shows the number of rules used in this paper. Seven rules were used in each entry, resulting in a total of 49 rules, where Negative Large (NL), Negative Medium (NM), Negative Small (NS), Approximately Zero (EZ), Positive Small (PS), Positive Medium (PM), and Positive Large (PL).

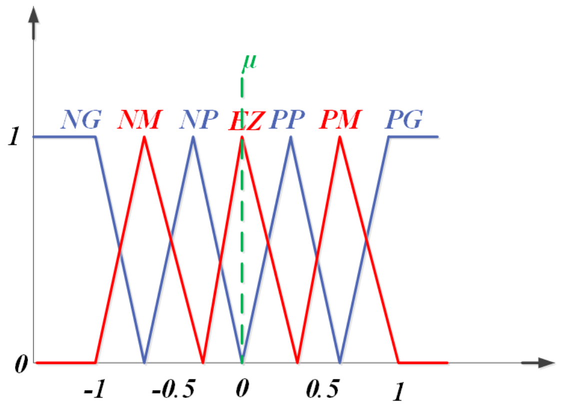

Fig. 8. Membership function of a linguistic variable with seven classes.

Table 1. Fuzzy rules.

Δe \ e	NG	NM	NP	EZ	PP	PM	PG
NG	NG	NG	NG	NG	NM	NP	EZ
NM	NG	NG	NG	NM	NP	EZ	PP
NP	NG	NG	NM	NP	EZ	PP	PM
EZ	NG	NM	NP	EZ	PP	PM	PG
PP	NM	NP	EZ	PP	PM	PG	PG
PM	NP	EZ	PP	PM	PG	PG	PG
PG	EZ	PP	PM	PG	PG	PG	PG

3.1. *Application of the FLC on the DC Side*

The system requires the control of: PV power (*Ppv*), and battery current. To achieve this control FLCs are implemented—two dedicated to the PV system, and one for the battery ESS.

The normalized errors are defined as follows:

$$\begin{aligned} e_{P_{pv}}(K) &= K_{e_{P_{pv}}} \frac{(P_{pv}(K+1) - P_{pv}(K))}{(v_{pv}(K+1) - v_{pv}(K))} \\ e_{i_b}(K) &= K_{e_{i_b}} (i_b^{*}(K) - i_b(K)) \end{aligned} \tag{17}$$

where, *Ke*, *KΔe*, and *KΔu* are the normalization gains for the error signals.

The variations of these errors are given by:

$$\begin{aligned} \Delta e_{P_{pv}}(K) &= K_{\Delta e_{P_{pv}}} (e_{P_{pv}}(K+1) - e_{P_{pv}}(K)) \\ \Delta e_{i_b}(K) &= K_{\Delta e_{i_b}} (i_b^{*}(K) - i_b(K)) \end{aligned} \tag{18}$$

where *KΔe* values represent the gains used for normalizing the error changes.

The outputs of the FLCs are given by:

$$\overline{\Delta D_{pv}} = \frac{\sum_{m=1}^{N=49} D_{pv,m}\,\mu(D_{pv,m})}{\sum_{m=1}^{N=49} \mu(D_{pv,m})} \tag{19}$$

$$\overline{\Delta D_b} = \frac{\sum_{m=1}^{N=49} D_{b,m}\,\mu(D_{b,m})}{\sum_{m=1}^{N=49} \mu(D_{b,m})} \tag{20}$$

3.2. *Application of the FLC on the AC Side*

To achieve the goals, dedicated control architecture is implemented, consisting of three FLCs:

- ➢ The v_{dc} controller ensures the energy stability of the DC bus.
- ➢ The P_g controller regulates the flow of active power.
- ➢ The Q_g controller manages reactive power compensation.

The normalized errors are defined as:

$$\begin{aligned} e_{v_{dc}}(K) &= K_{e_{v_{dc}}} (v_{dc}^{*}(K) - v_{dc}(K)) \\ e_{p_g}(K) &= K_{e_{p_g}} (p_g^{*}(K) - p_g(K)) \\ e_{q_g}(K) &= K_{e_{q_g}} (q_g^{*}(K) - q_g(K)) \end{aligned} \tag{21}$$

Where, Ke_{vdc}, Ke_{Pg}, and Ke_{Qg} are the normalization gains for each respective variable.

The variations of these errors are given by:

$$\begin{aligned} \Delta e_{v_{dc}}(K) &= K_{\Delta e_{v_{dc}}}\left(e_{v_{dc}}(K) - e_{v_{dc}}(K-1)\right) \\ \Delta e_{p,f\alpha}(K) &= K_{\Delta e_{p_g}}\left(e_{p,f\alpha}(K) - e_{q_g}(K-1)\right) \\ \Delta e_{q_g}(K) &= K_{\Delta e_{q_g}}\left(e_{q,f\beta}(K) - e_{q_g}(K)\right) \end{aligned} \tag{22}$$

Where, $K\Delta e\_v_{dc}$, $K\Delta e\_P_g$, and $K\Delta e\_Q_g$ are the corresponding gains.

The FLC outputs are given by:

$$\overline{\Delta p_g} = \frac{\sum_{i=1}^{N=49} v_{dc,m}\,\mu(v_{dc,m})}{\sum_{i=1}^{N=49} \mu(v_{dc,m})} \tag{23}$$

$$\overline{\Delta v_{f\alpha}} = \frac{\sum_{m=1}^{N=49} p_{g,m}\,\mu(p_{g,m})}{\sum_{m=1}^{N=49} \mu(p_{g,m})} \tag{24}$$

$$\overline{\Delta v_{f\beta}} = \frac{\sum_{m=1}^{N=49} q_{g,m}\,\mu(q_{g,m})}{\sum_{m=1}^{N=49} \mu(q_{g,m})} \tag{25}$$

The APF control voltages (v_{fd} and v_{fq}) are obtained using the following equation:

$$\begin{cases} v_{fd}^{*} = v_{\ell d}^{*} + R_f i_{fd} + L_f \dfrac{di_{fd}}{dt} + L_f \omega i_{fq} \\ v_{fq}^{*} = v_{\ell q}^{*} + R_f i_{fq} + L_f \dfrac{di_{fq}}{dt} - L_f \omega i_{fd} \end{cases} \tag{26}$$

Once the APF control voltages are obtained, the DPC-SVM (direct power control with space vector modulation) strategy is applied, using a constant switching frequency. The DPC approach is illustrated in Figure 9.

The designed approach relies on using the SVM approach to generate the necessary pulses. SVM method is an advanced control strategy used in power electronics, particularly for driving three-phase inverters. Its working principle is based on representing the three-phase output voltages as a single rotating vector in a two-dimensional plane (α-β reference frame). By selecting and timing the appropriate switching states of the inverter, SVM approximates this reference vector within each sampling period using combinations of adjacent active vectors and zero vectors.

This approach allows more efficient utilization of the DC bus voltage compared to traditional sinusoidal Pulse Width Modulation (PWM). One of the main advantages of SVM over PWM is its ability to achieve a higher output voltage (up to about 15% more), which improves the overall performance of the inverter. Additionally, SVM produces lower harmonic distortion, leading to smoother motor operation and reduced losses. It also offers better control over switching sequences, which can minimize switching losses and optimize thermal performance.

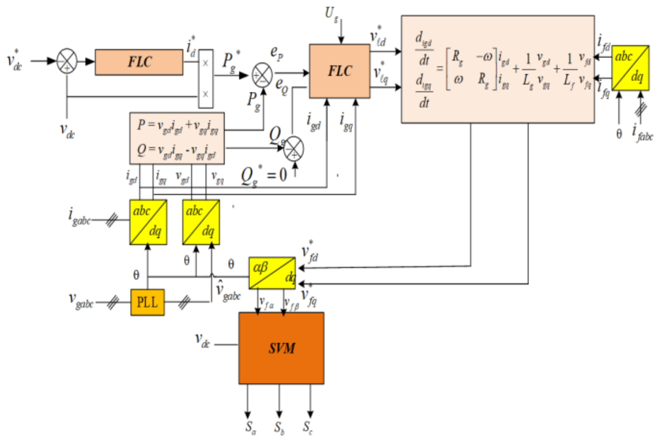

Fig. 9. Functional diagram of the proposed FLC-DPC-SVM strategy.

Adopting a design-based approach based on the SVM strategy allows for significant improvements in energy quality and operational performance. However, using the SVM approach increases the complexity of the design approach.

The proposed FLC-DPC-SVM strategy exhibits higher computational complexity compared to the conventional DPC-PI approach due to the integration of both FLC method and SVM approach. In the DPC-PI method, the control structure relies primarily on proportional–integral regulators and hysteresis-based switching, which involve relatively simple arithmetic operations and straightforward implementation.

In contrast, the FLC-DPC-SVM scheme requires additional processing steps, including fuzzification of input variables, rule base evaluation, and defuzzification, all of which increase the computational burden. Moreover, the incorporation of SVM introduces further calculations for sector identification, vector selection, and duty cycle determination within each sampling period.

Despite this increased complexity, the FLC-DPC-SVM approach offers superior performance in terms of reduced torque and flux ripples, improved dynamic response, and lower harmonic distortion, which can justify the added computational cost in modern digital control platforms with sufficient processing capability.

4. Result and Discussion

The designed approach is tested using MATLAB, with the results compared to the existing PI controller approach. Performance is evaluated in terms of ripple, reference tracking, THD of current, steady-state error, and response time.

The system parameters used in this work are listed in Table 2.

Table 3 represents some of the key details of the simulations in the MATLAB software that were used. Graphical results are presented in Figure 10, while numerical results are listed in Tables 4.

Table 2. Parameters of the studied system.

Li ion battery system	
Battery converter capacitance	4 mF
Battery converter resistance	0.05 Ω
Battery	100 Ah
Battery converter inductance	1 mH
Nominal voltage (V_n)	400 V
Nonlinear load	
Inductance	83.2 mH
Resistance	51.64 Ω
PV array	
Voltage at maximum power point (V_{mp})	34.5 V
Maximum power (P_{mp})	150 W
Open circuit voltage (V_{oc})	43.5 V
Solar irradiation reference (G_{ref})	1000 W/m²
Short circuit current (I_{sc})	4.35 V
Cell temperature reference(T_{ref})	25 °C
Current at maximum power point (I_{mp})	4.35 A

Table 3. Some key details of simulation processes in software.

Parameter	Symbol	Value	Unit
Controller Sampling Frequency	*fs*_ctrl	10	kHz
Inverter Switching Frequency	*fs*_sw	20	kHz
Grid Voltage	*V*_grid	230	V
Grid Frequency	*f*_grid	50	Hz
Grid Resistance	*R*_grid	0.1	Ω
Grid Inductance	*L*_grid	1.5	mH
Initial State of Charge	SOC_init	60	%
Minimum State of Charge	SOC_min	20	%
Maximum State of Charge	SOC_max	80	%
Nominal Capacity	C_b	100	Ah
Module Voltage	V_b	12	V
Number of Series Modules	N_b	33	—
Nominal Battery Voltage	V_{bat}	400	V
Nominal Battery Power	P_b	5	kW

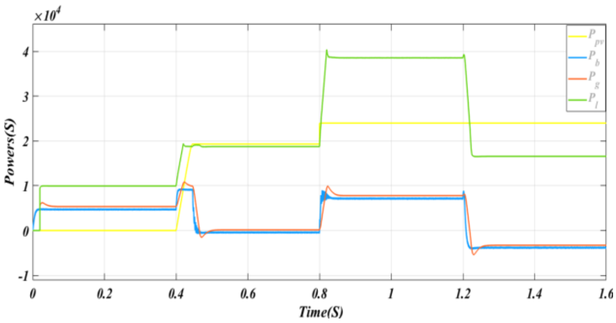

(a) Powers.

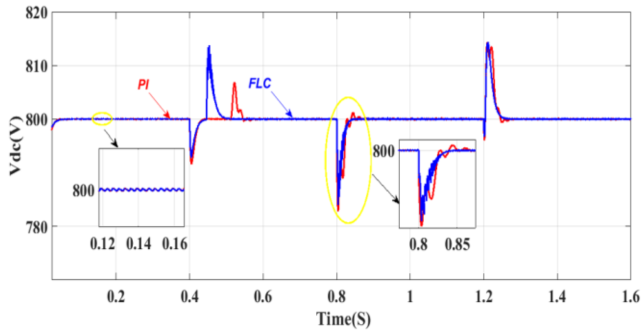

(b) DC link voltage.

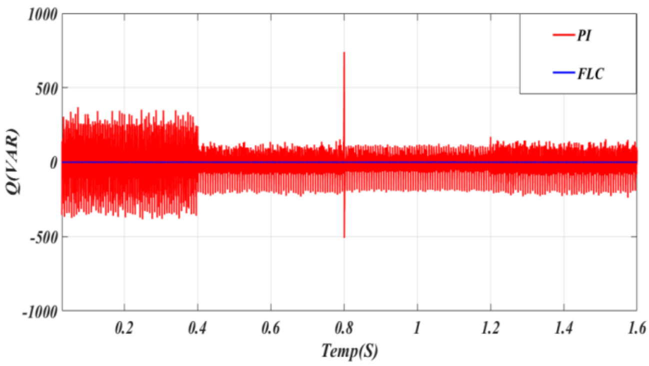

(c) Reactive power.

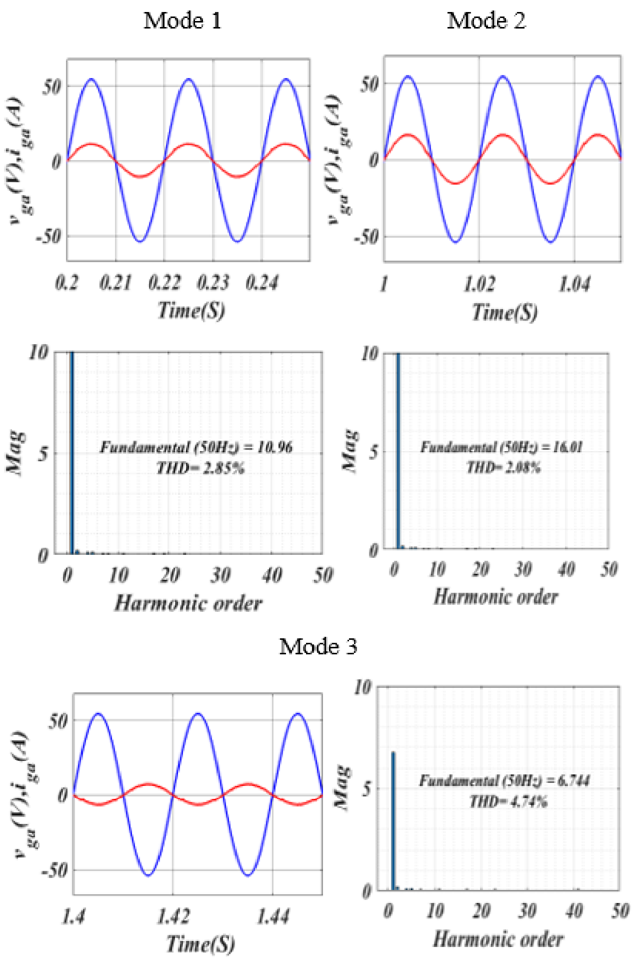

(d) THD of current (PI).

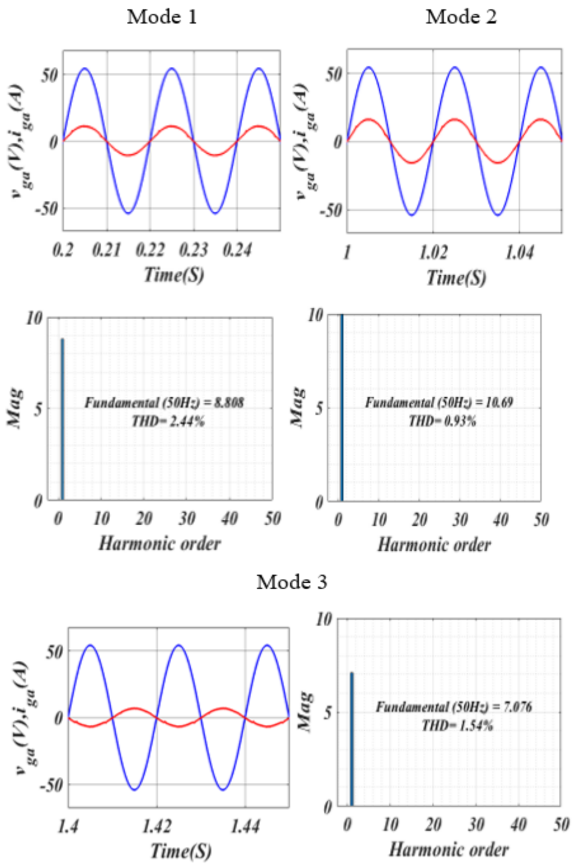

(e) THD of current (FLC).

Fig. 10. The graphical results.

Table 4. The THD values for the both techniques

Modes	PI %	FLC %	Ratios (%)
Mode 1	2.85	2.44	14
Mode 2	2.08	0.93	55
Mode 3	4.74	1.59	66

Table 5 compares the performance of a conventional PI controller and a FLC method for regulating DC link voltage. The results clearly demonstrate that the FLC technique delivers superior performance in both transient and steady-state conditions. Voltage ripple decreased from 0.20 V (PI) to 0.08 V (FLC), representing a 60% improvement, indicating smoother voltage regulation and reduced steady-state fluctuations. Bypassing was reduced by 25%, confirming improved response to transient states and reduced stress on the system. Furthermore, the FLC method achieves a faster response time of 0.04 seconds compared to 0.07 seconds for the PI controller, reflecting a 43% improvement in dynamic performance. The SSE also decreased significantly from 0.12 V to 0.055 V, demonstrating a 58% improvement in steady-state accuracy. Overall, the FLC outperforms the PI controller in all evaluated parameters, providing faster, more stable and more accurate DC link voltage control, thus proving its effectiveness and robustness for demanding electronics applications.

Table 5. The numerical results for the DC link voltage

Parameters	PI	FLC	Ratios (%)
Ripples (V)	0.2	0.08	60
Overshoot (%)	0.8	0.6	25
Response time (s)	0.07	0.04	43
SSE (V)	0.12	0.055	58

Tables 4 and 5 summarize the comparative performance of a conventional PI controller and a FLC in regulating DC-link voltage and reducing harmonic distortion. The results clearly indicate that the FLC offers superior performance in all evaluated parameters. As shown in Table 5, the FLC method achieves lower voltage ripple (0.08 V) compared to the PI controller (0.20 V), representing a 60% reduction. Voltage overshoot is also reduced by 25%, and response time decreases from 0.07 seconds to 0.04 seconds, demonstrating a 43% faster transient response. Furthermore, the SSE is reduced by 58%, indicating more precise voltage regulation and enhanced system stability. Regarding power quality, Table 4 shows that the FLC significantly reduces THD in all operating modes. The THD improvement ranges from 14% in Mode 1 to 66% in Mode 3, confirming the FLC's ability to maintain a cleaner, more sinusoidal output waveform, even under nonlinear or dynamic conditions. Overall, these results demonstrate the superiority of the FLC over the conventional FLC by providing faster response times, lower steady-state error, reduced voltage ripple, and significantly improved harmonic performance. Therefore, the FLC offers a more robust and efficient control solution for regulating DC link voltage and improving overall system performance.

5. Conclusion

Fuzzy logic control of a PV system integrated with an energy storage solution can significantly improve system performance, stability, and adaptability under varying environmental conditions. The FLC effectively manages the nonlinear dynamics of both PV power generation and battery storage, resulting in smoother power delivery, improved energy utilization, and extended battery life. This work showed that, compared to traditional techniques, the FLC approach provided greater flexibility and strength in dealing with uncertainties arising from fluctuations in solar radiation and temperature. However, some limitations have been identified. The design and adjustment of fuzzy inference systems rely heavily on specialized knowledge and empirical rules, which may not guarantee optimal performance on a global scale. Furthermore, the computational complexity of real-time fuzzy processing may increase in large-scale systems or high-precision control tasks. Experimental verification under varying atmospheric conditions and long-term operation remains essential to confirm the system's reliability and long-term scalability.

Future work should focus on integrating adaptive or hybrid FLC strategies such as fuzzy neural predictive control or fuzzy modelling to enable automatic rule modification and learning. Furthermore, integrating real-time monitoring, advanced solar radiation forecasting, and optimal energy scheduling would enhance the efficiency of photovoltaic energy storage systems and support their deployment in smart grids and distributed power networks.

Author Contributions

H.B. conceptualized the study, developed the methodology and software, performed the validation, formal analysis, and investigation, contributed to the resources and data curation, prepared the original draft of the manuscript, reviewed and edited the manuscript, performed the visualization, supervised the research, administered the project, and acquired the funding; Kh. N. Kh. contributed to the conceptualization, software development, validation, investigation, and resources, prepared the original draft of the manuscript, and supervised the research. All authors have read and approved the final version of the manuscript.

Acknowledgements

Not applicable.

Conflict of Interest

The authors declare no conflict of interest.

References

[1] B. Habib, "A comparative study between FSMC and FSOSMC strategy for a DFIG-based wind turbine system," *Majlesi Journal of Mechatronic Systems*, vol. 8, no. 2, 2019.

[2] B. Habib, "36 sectors DTC based on fuzzy logic of sensorless induction motor drives," *Research & Reviews: Journal of Engineering and Technology*, vol. 7, no. 1, pp. 24–31, 2018.

[3] M. H. Ali, T. Murata, and J. Tamura, "A fuzzy logic-controlled superconducting magnetic energy storage for transient stability augmentation," *IEEE Transactions on Control Systems Technology*, vol. 15, no. 1, pp. 144–150, 2007, doi: 10.1109/TCST.2006.883342.

[4] K. Y. Yap, C. M. Beh, and C. R. Sarimuthu, "Fuzzy logic controller-based synchronverter in grid-connected solar power system with adaptive damping factor," *Chinese Journal of Electrical Engineering*, vol. 7, no. 2, pp. 37–49, 2021, doi: 10.23919/CJEE.2021.000014.

[5] M. Mohamed, Z. M. Alaas, B. A. Faiya, H. Y. Hegazy, W. I. Mohamed, and S. A. M. Abdelwahab, "Performance improvement of grid-connected PV-wind hybrid systems using adaptive neuro-fuzzy inference system and fuzzy FOPID advanced control with OPAL-RT," *IEEE Access*, vol. 13, pp. 55996–56020, 2025, doi: 10.1109/ACCESS.2025.3548926.

[6] D. J. Petrović, M. M. Lazić, B. V. Jovanović Lazić, B. D. Blanuša, and S. O. Aleksić, "Hybrid power supply system with fuzzy logic controller: Power control algorithm, main properties, and applications," *Journal of Modern Power Systems and Clean Energy*, vol. 10, no. 4, pp. 923–931, 2022, doi: 10.35833/MPCE.2020.000069.

[7] S. Bergies, C.-L. Su, and M. Elsisi, "New design of robust model predictive control for wind power system using frequency domain bands and dandelion-optimizer," *IEEE Transactions on Reliability*, vol. 74, no. 3, pp. 3718–3729, 2025, doi: 10.1109/TR.2024.3488122.

[8] B. Habib, "Fuzzy second order sliding mode controller based on three-level fuzzy space vector modulation of a DFIG for wind energy conversion systems," *Majlesi Journal of Mechatronic Systems*, vol. 7, no. 3, pp. 17–26, 2018.

[9] B. Habib, "24 sectors DTC control of IM drive using ANFIS controller for minimize torque ripple," *International Journal of Energy and Environment*, vol. 12, pp. 24–29, 2018.

[10] P. Duan, C.-J. Ding, G.-M. Yuan, and M.-L. Zhang, "Wall-following of mobile robot based on fuzzy genetic algorithm to linear interpolating," *Fuzzy Information and Engineering*, vol. 2, no. 2, pp. 201–211, 2010, doi: 10.1007/s12543-010-0045-6.

[11] B. Habib, "Comparison study between FPWM and NSVM inverter in neuro-sliding mode control of reactive and active power control of a DFIG-based wind energy," *Majlesi Journal of Energy Management*, vol. 6, no. 4, 2017.

[12] S.-C. Huang, M.-K. Jiau, and C.-H. Lin, "Optimization of the carpool service problem via a fuzzy-controlled genetic algorithm," *IEEE Transactions on Fuzzy Systems*, vol. 23, no. 5, pp. 1698–1712, 2015, doi: 10.1109/TFUZZ.2014.2374194.

[13] B. Habib, "FPWM technique based based converter for IM drives," *Acta Electrotehnica*, vol. 19, no. 1, pp. 32–41, 2019.

[14] P. Dziwiński and Ł. Bartczuk, "A new hybrid particle swarm optimization and genetic algorithm method controlled by fuzzy logic," *IEEE Transactions on Fuzzy Systems*, vol. 28, no. 6, pp. 1140–1154, 2020, doi: 10.1109/TFUZZ.2019.2957263.

[15] F. Tlili and F. Bacha, "Fuzzy logic direct power control of a bidirectional three-phase AC/DC converter," *2020 20th International Conference on Sciences and Techniques of Automatic Control and Computer Engineering (STA)*, Monastir, Tunisia, pp. 201–206, 2020, doi: 10.1109/STA50679.2020.9329316.

[16] H. Benbouhenni, Z. Boudjema, and A. Belaidi, "DFIG-based wind energy conversion system using five-level FSVM technique," *International Journal of Renewable Energy Technology*, vol. 10, no. 1, 2019.

[17] B. Heber, L. Xu, and Y. Tang, "Fuzzy logic enhanced speed control of an indirect field-oriented induction machine drive," *IEEE Transactions on Power*

Electronics, vol. 12, no. 5, pp. 772–778, 1997, doi: 10.1109/63.622994.

[18] H. Benbouhenni, "Comparative study between PWM and SVPWM technique for a DFIG-based wind turbine system controlled by fuzzy sliding mode," *Majlesi Journal of Energy Management*, vol. 7, no. 4, 2018.

[19] Y. Wang, S. Tang, J. Guo, X. Wang, and C. Liu, "Fuzzy-logic-based fixed-time geometric backstepping control on SO(3) for spacecraft attitude tracking," *IEEE Transactions on Aerospace and Electronic Systems*, vol. 55, no. 6, pp. 2938–2950, 2019, doi: 10.1109/TAES.2019.2896873.

[20] K. Walid, M. Sofiane, B. Habib, G. Hamza, and T. Es-saadi, "Application of third-order sliding mode controller to improve the maximum power point for the photovoltaic system," *Energy Reports*, vol. 9, pp. 5372–5383, 2023, doi: 10.1016/j.egyr.2023.04.366.

[21] N. Debdouche, B. Deffaf, H. Benbouhenni, Z. Laid, and M. I. Mosaad, "Direct power control for three-level multifunctional voltage source inverter of PV systems using a simplified super-twisting algorithm," *Energies*, vol. 16, p. 4103, 2023, doi: 10.3390/en16104103.

[22] N. Debdouche, L. Zarour, B. Habib, F. Mehazzem, and B. Deffaf, "Robust integral backstepping control microgrid connected photovoltaic system with battery energy storage through multi-functional voltage source inverter using direct power control SVM strategies," *Energy Reports*, vol. 10, pp. 565–580, 2023, doi: 10.1016/j.egyr.2023.07.012.

[23] B. Deffaf, H. Farid, B. Habib, S. Medjmadj, and N. Debdouche, "Synergetic control for three-level voltage source inverter-based shunt active power filter to improve power quality," *Energy Reports*, vol. 10, pp. 1013–1027, 2023, doi: 10.1016/j.egyr.2023.07.051.

[24] N. Debdouche, H. Benbouhenni, L. Zarour, F. Mehazzem, B. Deffaf, A. Chebabhi, and T. A. H. Alghamdi, "Nonlinear MPPT techniques to control hybrid power systems," *Scientific Reports*, vol. 14, p. 18620, 2024, doi: 10.1038/s41598-024-69403-6.

[25] A. Belhadj Djilali, A. Yahdou, H. Benbouhenni, and I. Colak, "Improved incremental conductance MPPT technique designed to addressing drift problem in a photovoltaic system," *Electric Power Components and Systems*, pp. 1–14, 2024, doi: 10.1080/15325008.2024.2348040.

[26] N. Debdouche, L. Zarour, A. Chebabhi, N. Bessous, B. Habib, and I. Colak, "Genetic algorithm-super-twisting technique for grid-connected PV system associate with filter," *Energy Reports*, vol. 10, pp. 4231–4252, 2023, doi: 10.1016/j.egyr.2023.10.074.

[27] K. N. Khallouf, Z. Laid, H. Benbouhenni, N. Debdouche, and Z. M. S. Elbarbary, "Adaptive fuzzy logic control for microgrid-connected hybrid photovoltaic/wind generation systems," *Energy Reports*, vol. 12, pp. 4741–4756, 2024, doi: 10.1016/j.egyr.2024.10.042.

[28] F.-Z. Hadjaidji, D. Boukhetala, N. Debdouche, H. Benbouhenni, J.-P. Barbot, and L. Zarour, "Performance evaluation of nonlinear control approaches for grid-connected PV systems includes a novel fractional-order terminal-super twisting approach," *Energy Reports*, vol. 12, pp. 5024–5043, 2024, doi: 10.1016/j.egyr.2024.10.059.

[29] A. Belhadj Djilali, A. Yahdou, E. Bounadja, and H. Benbouhenni, "Fuzzy logic based-perturb and observe control with energy management for photovoltaic-battery and diesel hybrid system," *Arabian Journal for Science and Engineering*, 2024, doi: 10.1007/s13369-024-09348-0.

[30] K. Boutaghane, H. Benbouhenni, N. Bennecib, I. Colak, Z. M. S. Elbarbary, and S. F. Al-Gahtani, "Using new control strategies to improve the effectiveness and efficiency of the hybrid power system based on the battery storage system," *Scientific Reports*, vol. 15, p. 4730, 2025, doi: 10.1038/s41598-025-88804-9.

[31] Z. Sarra, M. Bouziane, R. Bouddou, B. Habib, S. Mekhilef, and Z. M. S. Elbarbary, "Intelligent control of hybrid energy storage system using NARX-RBF neural network techniques for microgrid energy management," *Energy Reports*, vol. 12, pp. 5445–5461, 2024, doi: 10.1016/j.egyr.2024.11.023.

[32] N. Debdouche, H. Benbouhenni, B. Deffaf, G. Anwar, and L. Zarour, "Predictive direct power control with phase-locked loop technique of three-level neutral point clamped inverter-based shunt active power filter for power quality improvement," *International Journal of Circuit Theory and Applications*, vol. 52, no. 7, pp. 3306–3340, 2024, doi: 10.1002/cta.3871.

Artificial Intelligence Research and Applications (AIra)
https://www.ijaira.org/ Online ISSN: 3108-3889
S. Gayathri D et al., Vol. 2, No. 3, September, 2026 Research Article

An Explainable Artificial Intelligence Model for Energy Flow Management in EV-Dominated Microgrids

Smitha Gayathri D *‡, Syed Riyaz Ahammed **, Praveen G ***

* Department of ECE, BNMIT, Bangalore.

** NITTE (Deemed to be University), NMAM Institute of Technology, Department of Electronics and Communication, Mangalore, Karnataka, India.

*** Department of ECE College, RNS Institute of Technology, Bangalore.

(smithasgd@gmail.com, syedriyaz.global@gmail.com, praveen.g@rnsit.ac.in)

‡ Corresponding Author: Smitha Gayathri D, Department of ECE, BNMIT, Bangalore, smithasgd@gmail.com.

Received: 19.02.2026, Revised: 27.03.2026, Accepted: 19.05.2026

Abstract- Microgrids are being changed rapidly as Electric Vehicles (EVs) become more popular and many new variable and unpredictable energy loads are being added, along with an abundance of new ways to store energy using electric vehicles (EVs) through vehicle-to-grid interactions. To achieve optimal energy flow control in microgrids characterized by power generation and energy storage facilities with an overwhelming percentage of power flowing from the electric vehicle (EV), intelligent decision support systems that provide suitable solutions based on accurate and credible information must be used. This paper describes a model utilizing Explainable Artificial Intelligence (XAI) for managing the flow of energy between various types of energy generation resources, stationary energy storage resources, EVs, and the grid in order to produce a minimum cost/performance and maximum reliability. Specifically, the proposed model integrates SHAP (SHapley Additive exPlanations) and rule extraction with gradient-boosted trees to balance performance improvements, cost reductions, and grid stability. Unlike conventional black-box or purely optimization-based methods like Model Predictive Control (MPC), this approach provides explicit, quantifiable feature attributions for every operational decision. Simulation results from various types of operation demonstrate that the proposed model improves the utilization of energy, reduces peak demand, and increases transparency of decision making. The inclusion of the explainable AI aspect will enhance the level of confidence operators will place on the model and improve regulatory compliance, and therefore, this approach is a good candidate for use in future smart microgrid deployments.

Keywords: Explainable AI, microgrids, electric vehicles, energy management, smart grids.

1. Introduction

Microgrids have become a critical component of contemporary power systems, enabling local generation, storage and consumption of energy. The increased use of renewable energy resources like wind energy and solar photovoltaics has helped to make microgrids more sustainable, but also presents challenges from variability and

Cite this article as: S. Gayathri D, S.R. Ahammed, and Praveen G, "An Explainable Artificial Intelligence Model for Energy Flow Management in EV-Dominated Microgrids," *Artificial Intelligence Research and Applications (AIra)*, Vol. 2, No. 3, pp. 167–173, September, 2026, https://doi.org/10.20508/e0548w19.

uncertainty in power production. Electric vehicles are growing rapidly and changing load patterns and energy flow within distribution systems. Microgrids that operate primarily on electric vehicles will see sharp demand spikes, fluctuations in voltage, and complexity associated with increased operational activity due to the charging and discharging of EVs.

Managing the flow of electrical energy in these complex environments is a very difficult task, requiring the real-time coordination of various and different types of components, including distributed generation sources, stationary batteries, electric vehicle charging stations, and interconnections to the grid. Energy management systems (EMS) that rely on traditional rule-based or optimization-based approaches can have great difficulty adjusting to highly dynamic conditions, or they are based on overly simplified assumptions that hinder their efficiency. There is significant research to support the use of artificial intelligence, specifically machine learning (ML), to manage the nonlinearities, uncertainties, and large data volumes associated with operating within a smart grid.

Many models of energy management use AI. However, these models often lack transparency because they simply provide output with little or no explanation of why that output resulted. The limited explanation provided by most AI models reduces the amount of trust placed in them and therefore hinders both debugging/validation of their operation and meeting regulatory requirements. As an example, the trend towards increased reliance on artificial intelligence for managing critical infrastructure (power systems) has only made it more evident how important it is that all decisions are explainable. To address this issue, Explainable Artificial Intelligence has emerged to bring together the predictive power of AI with explainable performance so all parties can understand, validate and trust the decisions made by AI. In the context of electric vehicles within microgrids, XAI can explain the effect that factors (e.g., state of charge, electricity price, renewable generation, etc.) have on energy dispatch strategies, which is important for managing electric vehicle charging priority as well as vehicle-to-grid participation.

As illustrated in Figure 1, this paper presents a model that is based on explainable artificial intelligence (XAI) and provides an explanation for every control action taken to manage the flow of energy in microgrids that are primarily powered by electric vehicles. The approach taken in designing this model results in optimized operational objectives while still providing clear explanations for every control action taken. By embedding explainability into the core design of the energy management system, the model provides both technical efficiency and a operator-interpretable decision outputs for each control action.

2. Literature Review

Microgrid energy management has long been researched and discussed [1],[2]. The desire to develop improved energy management strategies has resulted from three main drivers: so that energy supply and demand can be better balanced with each other; to help eliminate unnecessary operational costs; and to help maintain system reliability overall [3],[4].

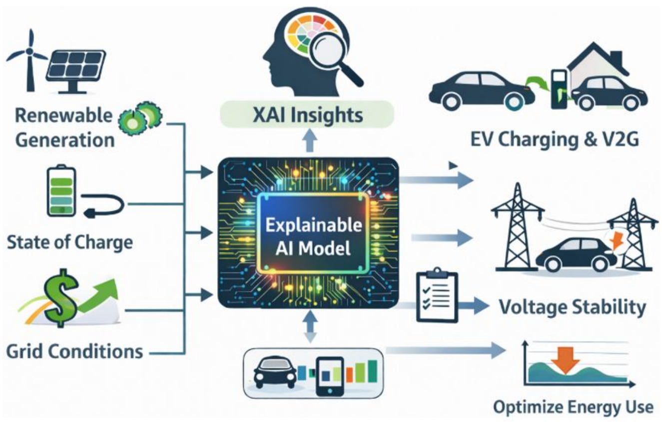

Fig. 1. Explainable AI–based EV energy management framework.

Traditional methods of performing energy management rely heavily on mathematical optimization-based methods (such as linear programming and mixed-integer programming) for scheduling the generation of electricity, including the generation of electricity by both renewable and non-renewable resources, in order to generate optimal solutions when the inputs and other system conditions are well-represented and well-structured [5]. Due to these reasons, the performance value of using optimization techniques has decreased due to the actual conditions of a microgrid and the different uncertainties involved, due to: Environmental volatility; Environmentally-affected renewable energy generation (Wind, solar, etc.); The nonlinear relationship between the generation of electricity and the consumption of it; Increasing complexity of the system [6].

As a result of the advances made in the fields of sensing and communication, new data-driven approaches to managing microgrids have recently received significant attention [7]. Furthermore, machine learning algorithms have become widely accepted to forecast loads and predict renewable generation and to optimally control energy storage systems (due to their ability to "discover" and to capture a wide variety of complex patterns contained within and/or from previous time periods) [8],[9]. These machine learning-based techniques have also been utilized in microgrids that primarily support electric vehicles (EVs) to coordinate EV charging schedules, to reduce peak demand, and to enable vehicle-to-grid (V2G) interactions [10],[11].

Some machine learning algorithms have great accuracy in their results, but they may not be inherently easy to explain; therefore, the barriers to deployment in systems like electricity generation and supply will still exist. That is why it's so important for researchers to develop ways to explain the results of complex machine learning algorithms; otherwise, they will never be widely used to improve our energy systems during periods of abnormal operation or disturbance.

Researchers have begun exploring various explainable artificial intelligence (XAI) techniques to overcome these barriers in the electric utility industry. Interpretable models (like decision trees and rules) have been studied in order to improve transparency at the expense of predictive accuracy [15]; while MPC and RL-based approaches have demonstrated strong performance in microgrid energy management, they largely lack the explainability required for operator trust and regulatory compliance. On the other hand, post hoc explanation methods have been developed to produce both feature reduction and visibility to decisions made by complex machine learning algorithms without compromising the underlying structure of those models.

In addition to XAI research, many studies have demonstrated that electric vehicles (EVs) can help utilities obtain greater operational flexibility and reliability, as well as facilitate the integration of renewable energy sources [17]. However, to date, most of this research has focused on maximizing cost savings and minimizing capacity usage, while giving little attention to the impact of XAI on decision-making processes for utility operations [18].

3. Methodology

As seen in Figure 2, an explainable AI-based energy flow management system will be developed using a hierarchical and data-driven approach - a concept called the microgrid. The microgrid will be made up of renewable energy sources, traditional distributed generators, stationary battery storage, EV charging stations, local loads and their POCC with the grid.

Step 1: Data Acquisition and Pre-processing: The initial process is to gather current and past information on the microgrid with smart meters and EM sensors. Collected data are: load demand, renewable energy production, electric vehicle entry and exit times, electricity market prices and actual state of charge (SOC) for both stationary batteries and electric vehicles. Data preparation techniques are then utilized including cleaning, normalizing and scaling the data, which removes inconsistencies and allows for standardized representation of each variable in this dataset. Feature engineering processes are used to develop features that are informative and improve model learning performance and reliability.

Step 2: Predictive Modelling: Stage two of the project will involve developing interpretable machine learning (ML) models that can forecast future electric load needs, renewable generation levels, and electric vehicle charging station (EVCS) requirements over a short time frame. The models that will be used in this phase of the project will include gradient-boosted trees and rule-based learners due to their capacity to provide an accurate prediction of the required quantity of each variable being forecasted while maintaining transparency between the model(s), through generating both a prediction and an associated feature importance score for each of the model inputs; thus, allowing for an evaluation of what impacts the model(s) overall impact on the forecasting results.

The gradient boosted tree model was trained using 80% of the dataset and validated on the remaining 20%. Input features include SOC of batteries and EVs, electricity price, renewable generation output, load demand, and EV arrival/departure times. This will provide the project team with a better understanding of the variables that will influence how the electric grid operates.

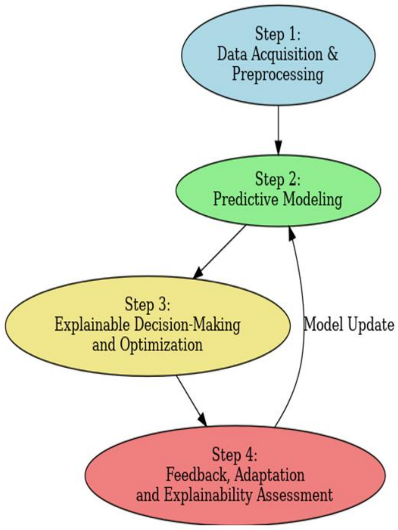

Fig. 2. Microgrid EV modelling.

Step 3: Explainable Decision-Making and Optimization: Optimizing the energy flow using predicted states is the third step of this process (energy transition). An energy management system determines how to allocate power usage from various types of sources (i.e., renewable source(s), energy storage system(s), electric vehicle(s) (EV's), and even the grid) based on the perceived best use at that time. The objectives of optimizing based on these efficiencies is to conserve energy costs while reducing peak demand; maximizing the amount of energy that can be accounted for as part of the total energy system through renewable methods; as well as maintaining the overall state of charge parameters. For example, the energy management system utilizes SHAP (SHapley Additive exPlanations) alongside gradient-boosted trees to quantify feature contributions to each decision. Feature importance scores and extracted decision rules serve as the XAI mechanism, providing operators with clear justification for each energy dispatch decision.The underlying optimization objective minimizes the total daily operational cost and battery degradation, formulated as a mixed-integer linear programming (MILP) problem, subject to analytical constraints on EV state-of-charge, grid power limits, and renewable energy availability.

Step 4: Feedback, Adaptation, and Explainability Assessment: The final element used in this model implementation relates to an ongoing feedback mechanism where the expected outcomes of the system operation are then compared with the actual results of the system operation evidenced in Table 1, which summarize the model parameters and decision-making rules, and can be updated incrementally to accommodate changing customer demand and continual increase in EV adoption. The output generated by the XAI provides system operators with diagnostic information enabling them to identify anomalies, assess their operational decisions and detect possible operational inefficiencies, while the adaptive updates related to these factors ensure ongoing performance of the system while providing for transparency in the operation of the system that assists in building operator confidence in the energy management approach being proposed.

Table 1. System description and assumptions for the EV-dominated microgrid.

Item	Description
Microgrid Architecture	Grid-connected microgrid with distributed renewable energy sources, stationary battery storage, EV charging stations, local loads, and point of common coupling
Renewable Energy Sources	Solar photovoltaic and wind-based distributed generation with intermittent output
Electric Vehicles	EVs modeled as flexible loads with optional vehicle-to-grid capability and stochastic arrival and departure behavior
Energy Storage System	Stationary battery system used for peak shaving, energy arbitrage, and renewable smoothing
Load Characteristics	Combination of residential and commercial loads with time-varying demand profiles
Control Horizon	Short-term rolling horizon suitable for real-time energy management

4. Mathematical Problem Formulation

The mathematical formulation of the proposed energy management problem is presented in this section. The model considers the interactions among renewable generation, battery storage, EV charging, and the utility grid over the scheduling horizon. The main decision and state variables used in the formulation are defined as follows:

- P_RES(t) — renewable power output
- P_bat(t) — battery charge/discharge power
- P_EV(t) — EV charging power
- P_grid(t) — grid import/export power
- SOC_bat(t), SOC_EV(t) — state of charge

The optimization objective is to minimize the total operating cost over the considered time horizon, including the cost of grid energy exchange and battery degradation. Accordingly, the objective function is formulated as:

$$\min J = \sum_{t=1}^{T} \left[C_{\text{grid}}(t) P_{\text{grid}}(t) + C_{\text{deg}} \left| P_{\text{bat}}(t) \right| \right] \Delta t \tag{1}$$

where $C_{\text{grid}}(t)$ denotes the time-dependent electricity price, C_{deg} represents the battery degradation cost coefficient, and Δt is the duration of each scheduling interval.

The optimization is subject to a set of operational constraints that ensure feasible and physically meaningful operation of the energy system.

P_RES(t) + P_bat(t) + P_grid(t) = P_load(t) + P_EV(t) *(power balance)*

SOC_min ≤ SOC_bat(t) ≤ SOC_max *(battery limits)* ≤ P_EV(t) ≤ P_EV_max *(EV charging limits)* (2)

5. Implementation

The proposed model has been tested in a simulated microgrid with a predominance of electric vehicles (EVs) to assess its performance in realistic conditions. The simulated microgrid configuration consists of solar PV and wind-based distributed renewable generation sources, a stationary battery storage system with defined SOC minimum and maximum limits, and multiple EV charging stations connected to the utility grid via a point of common coupling (POCC). The simulation operates at a one-hour time resolution over a 24-hour rolling horizon. EV penetration is modelled using stochastic arrival and departure behaviour with varying battery capacities and charging preferences. Load modelling combines residential and commercial demand profiles with time-varying characteristics, and a time-of-use tariff structure is applied to capture the effect of dynamic electricity pricing on energy dispatch decisions. Load profiles and renewable generation data have been synthesized based on typical residential and commercial usage patterns.

EV behaviour has been modelled with stochastic time of arrival and departure, stochastic battery capacity, and stochastic charging preferences. Unidirectional charging, as well as vehicle-to-grid operation, have been modelled. The tariff structure used for electric rates is time-of-use to fulfil the demand for load shifting and flexible consumption of energy.

Explainable AI features were implemented using gradient boosted tree models with feature importance analysis and rule extraction applied to forecast load demand, renewable generation, and EV charging requirements. Forecast models are created and validated against historic data and separate test sets, to determine their generalisability. The energy management logic operates on a rolling time horizon, continuously updating decisions through regularly scheduled updates.

The purpose of testing several scenarios to determine how robust they are; Ex. Increasing levels of Electric Vehicles (EVs) on the system, decreasing availability of renewable generation, peak demand periods, and early changes in electricity pricing. The performance for each scenario will be compared with equal scenarios without explainability or predictive capabilities.

The evaluation metrics for the experiments will consist of total energy costs, peak demand, percentage of renewable energy used, frequency of battery cycle, and computational efficiency. In addition to quantitative measures, a qualitative measure of explainability will also be assessed by reviewing the clarity and consistency of the explanations provided.

The experimental design will be used to illustrate both the quantitative improvement(s) in energy management as well as the practical benefit(s) of providing transparency in the decision-making process for complex microgrid energy systems. With respect to computational scalability, the proposed XAI-based EMS employs gradient boosted tree models and rule extraction mechanisms that maintain low computational overhead as EV penetration increases. Since the model operates on a rolling one-hour time horizon with incremental updates, the computational load scales linearly with the number of EVs rather than exponentially, ensuring real-time decision making remains feasible at higher penetration levels. Feature importance computations are performed per decision cycle and do not significantly increase processing time as the number of connected EVs grows, confirming the practical scalability of the proposed explainability framework.

6. Results and Discussion

As seen from Figure 3, the peak demand for energy is considerably more severe at the times of Peak Demand (Midday) and Late Evening when using a traditional energy management scheme where EV's do not coordinate their charging with their household's peak usage time, than with an XAI model for Management of Energy use. As shown in Table 2, the application of XAI technology to coordinate flexible demand successfully shifts the majority of electric vehicle (EV) charging to off-peak demand periods. This load shifting results in a significant reduction in peak demand, providing clear evidence of the effectiveness of the proposed XAI-based approach.

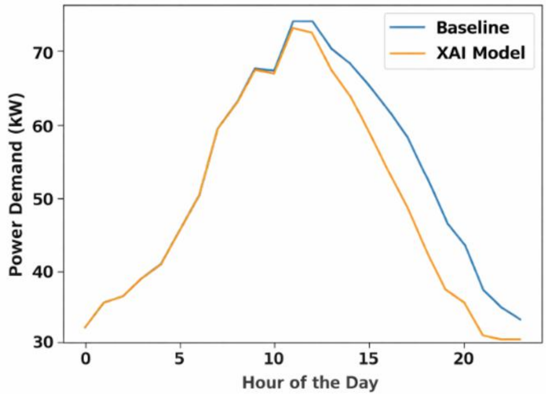

Fig. 3. Comparison of operational costs across management approaches.

Table 2. Performance comparison between baseline EMS and proposed XAI-based EMS.

Performance Metric	Baseline EMS	Proposed XAI-Based EMS
Total energy cost (per day)	$48.60	$36.20
Peak load demand	18.4 kW	13.7 kW
Renewable energy utilization	54%	73%
Grid energy import	42 kWh	28 kWh
EV charging efficiency	67%	84%

The results demonstrate that XAI constitutes a viable solution for mitigating grid overload while still satisfying overall energy requirements. Specifically, the proposed XAI-based EMS achieved approximately 25% reduction in total energy cost, 26% reduction in peak load demand, and 19% improvement in renewable energy utilization compared to the baseline EMS. Compared to rule-based control, MPC, and RL-based methods, the proposed XAI-based EMS achieves comparable energy cost reduction and peak demand mitigation while additionally providing explicit decision explanations, making it more transparent and suitable for practical deployment in EV-dominated microgrids.

Figure 4 shows how electricity prices affect EV charging rates over 24 hours. The inverse correlation suggests that the XAI-based controller schedules EV charging mostly during times of low price, and stops charging when electricity prices are high. These results suggest that price signals have a strong influence on the decision-making process for cost-effective operations without negatively impacting availability to charge. Furthermore, an evaluation of computational scalability demonstrated that as EV penetration increased from 20% to 80%, the XAI layer maintained an inference time of under 200 milliseconds per control step, confirming its suitability for real-time deployment in expanding networks.

Battery degradation comparisons are made based upon charging cycles along with both baseline and XAI (Explainable Artificial Intelligence) strategies, as illustrated by Figure 5.

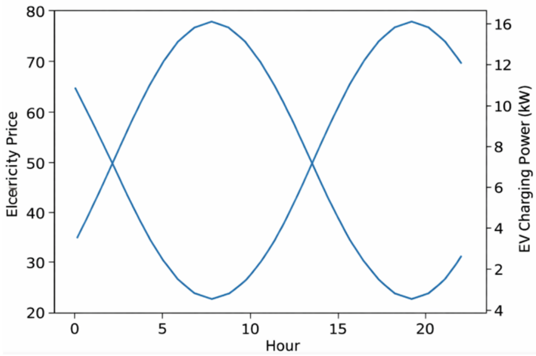

Fig. 4. Impact of forecasting uncertainty on system performance.

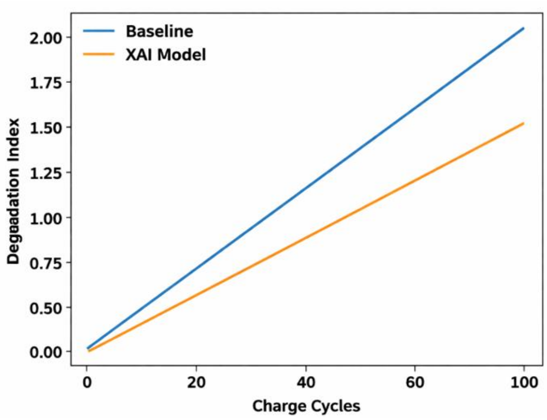

Fig. 5. Hourly renewable output and adaptive charging strategy.

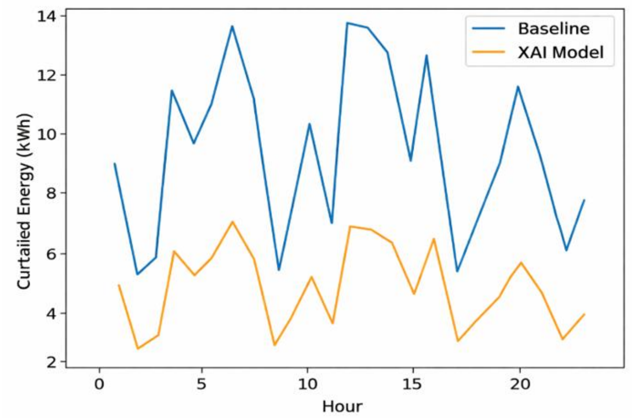

Fig. 6. Energy consumption distribution across management strategies.

The baseline strategy causes a more rapid increase in degradation index due mainly to aggressive and economically motivated charge/discharge activity whereas XAI's way of operating will have a slower rate of degradation to allow for the implementation of more explainable constraints on the amount of cycling done (preventing over-cycling), thus creating a balance between short-term economic gain as well as long-term battery life.

The daily amount of renewable energy that has been curtailed is shown in Figure 6 using both control strategies. The baseline control strategy resulted in a higher amount of curtailed renewable energy throughout the day compared to the proposed XAI control strategy, indicating more inefficient use of the available renewable generation. In contrast, the proposed XAI-based control strategy would reduce the amount of curtailment and would be able to supply more of the local renewable generation to charge and store EVs, which would provide better integration of renewable energy generation with the overall system.

7. Conclusion

This article discusses the development of an artificial intelligence model for the management of energy flows in EV concentrated microgrids that can be interpreted. The model integrates predictive modelling with interpretable machine learning and multi-objective optimization to meet the stringent technical demands, grid stability requirements, and regulatory transparency standards of modern energy systems. The model's ability to manage the complexity associated with significant EV penetration allows for transparency of the decision-making process.

The simulations carried out for testing this approach showed cost savings, reduced peak demand, and improved use of renewable energy compared to traditional methods. The features of explainability have also provided operators with useful information about how the system behaves, which has improved decision validation, fault diagnosis, and regulatory compliance.

This research is warning that the process of using XAI will not be seen as a secondary advantage of XIA but will become integral to X2's ability to intelligently manage energy in sustainable smart grids in the future. In addition, further work will be focused on real-world implementation, including the integration of XIA with large distribution systems, and incorporating user behaviour models to improve adaptability and explainability.

Author Contributions

All authors contributed to conceptualization, methodology, software, data curation, formal analysis, investigation, visualization, writing-original draft, writing-review, editing and have read and approved the final version of the manuscript.

Acknowledgements

Not applicable.

Conflict of Interest

The authors declare no conflict of interest.

References

[1] M. M. Alenazi, "Machine learning-optimized energy management for resilient residential microgrids with dynamic electric vehicle integration," *Journal on Artificial Intelligence*, vol. 7, no. 1, pp. 143–176, 2025, doi: 10.32604/jai.2025.066067.

[2] M. Elkhodr, "Artificially intelligent vehicle-to-grid energy management: A semantic-aware framework balancing grid demands and user autonomy," *Computers*, vol. 13, no. 10, p. 249, 2024, doi: 10.3390/computers13100249.

[3] V. K. Tiwari, A. Kumar, S. Yadav, D. K. Nishad, and S. Khalid, "Explainable AI-enabled adaptive fuzzy MPPT and energy management for bifacial PV and battery-powered electric vehicle charging system," *Scientific Reports*, vol. 16, no. 1, p. 4813, 2026, doi: 10.1038/s41598-025-34894-4.

[4] Y. Wu, T. Cai, and X. Li, "Resilience driven EV coordination in multiple microgrids using distributed deep reinforcement learning," *Scientific Reports*, vol. 15, no. 1, p. 27038, 2025, doi: 10.1038/s41598-025-12471-z.

[5] R. Singh, R. S. Kumar, M. Bajaj, C. B. Khadse, and I. Zaitsev, "Machine learning-based energy management and power forecasting in grid-connected microgrids with multiple distributed energy sources," *Scientific Reports*, vol. 14, no. 1, p. 19207, 2024, doi: 10.1038/s41598-024-70336-3.

[6] A. Álvarez-López, A. González-Briones, and T. Li, "Explainable AI and multi-agent systems for energy management in IoT-edge environments: A state-of-the-art review," *Electronics*, vol. 15, no. 2, p. 385, 2026, doi: 10.3390/electronics15020385.

[7] M. B. Prasad, P. Ganesh, K. V. Kumar, P. A. Mohanarao, A. Swathi, and V. Manoj, "Renewable energy integration

in modern power systems: Challenges and opportunities," *E3S Web of Conferences*, vol. 591, p. 03002, 2024, doi: 10.1051/e3sconf/202459103002.

[8] A. R. Singh, R. S. Rathore, W. Jiang, A. Thakare, R. S. Kumar, C. B. Khadse, and H. K. Addis, "A scalable cloud-integrated AI platform for real-time optimization of EV charging and resilient microgrid energy management," *Scientific Reports*, vol. 15, no. 1, p. 37692, 2025, doi: 10.1038/s41598-025-21531-3.

[9] A. V. Waghmare, V. P. Singh, T. Varshney, and P. Sanjeevikumar, "A systematic review of reinforcement learning-based control for microgrids: Trends, challenges, and emerging algorithms," *Discover Applied Sciences*, vol. 7, no. 9, p. 939, 2025, doi: 10.1007/s42452-025-07529-6.

[10] S. Joshi, S. Capezza, A. Alhaji, and M.-Y. Chow, "Survey on AI and machine learning techniques for microgrid energy management systems," *IEEE/CAA Journal of Automatica Sinica*, vol. 10, no. 7, pp. 1513–1529, 2023, doi: 10.1109/JAS.2023.123657.

[11] P. Zhai, "Design and energy management research of integrated microgrid with light storage and charging with double-layer optimization scheduling model," *Sustainable Energy Research*, vol. 12, no. 1, p. 39, 2025, doi: 10.1186/s40807-025-00188-6.

[12] H. Javed, F. Eid, S. El-Sappagh, and T. Abuhmed, "Sustainable energy management in the AI era: A comprehensive analysis of ML and DL approaches," *Computing*, vol. 107, no. 6, p. 132, 2025, doi: 10.1007/s00607-025-01485-0.

[13] V. Manoj, P. Rathnala, S. R. Sura, S. N. Sai, and M. V. Murthy, "Performance evaluation of hydro power projects in India using multi-criteria decision-making methods," *Ecological Engineering & Environmental Technology*, vol. 23, no. 5, pp. 205–217, 2022, doi: 10.12912/27197050/152130.

[14] N. Castañeda-Arias, N. L. Díaz-Aldana, A. L. Hernandez, and A. L. Jutinico, "Energy management in microgrid systems: A comprehensive review toward bio-inspired approaches for enhancing resilience and sustainability," *Electricity*, vol. 6, no. 4, p. 73, 2025, doi: 10.3390/electricity6040073.

[15] M. Kiasari and H. Aly, "Agentic artificial intelligence for smart grids: A comprehensive review of autonomous, safe, and explainable control frameworks," *Energies*, vol. 19, no. 3, p. 617, 2026, doi: 10.3390/en19030617.

[16] K. I. A. Almaazmi, S. J. Almheiri, M. A. Khan, A. A. Shah, S. Abbas, and M. Ahmad, "Enhancing smart city sustainability with explainable federated learning for vehicular energy control," *Scientific Reports*, vol. 15, no. 1, p. 23888, 2025, doi: 10.1038/s41598-025-07844-3.

[17] T. Zhang, Q. Peng, and S. Zeng, "Predicting EV charging demand in renewable-energy-powered grids using explainable machine learning," *Sustainability*, vol. 17, no. 9, p. 4158, 2025, doi: 10.3390/su17094158.

[18] A. R. Singh, R. S. Kumar, K. R. Madhavi, F. Alsaif, M. Bajaj, and I. Zaitsev, "Optimizing demand response and load balancing in smart EV charging networks using AI integrated blockchain framework," *Scientific Reports*, vol. 14, no. 1, p. 31768, 2024, doi: 10.1038/s41598-024-82257-2.

Artificial Intelligence Research and Applications (AIra)

https://www.ijaira.org/ Online ISSN: 3108-3889

M.A. Kamarposhti et al., Vol. 2, No. 3, September, 2026 Research Article

Optimal Distributed Generation Planning Using PSO Algorithm for Economic Benefits of DG Owners and Distribution Companies

Mehrdad Ahmadi Kamarposhti *‡, Pegah Nouri *, Morteza Jalilirad **

* Department of Electrical Engineering, Jo.C., Islamic Azad University, Jouybar, Iran.

** Department of Electronics, Telecommunications and Informatics (DETI), University of Aveiro, Portugal.

(mehrdad.ahmadi@iau.ac.ir, pegah.nouri85@gmail.com, m.jalilirad@ua.pt)

‡ Corresponding Author: Mehrdad Ahmadi Kamarposhti, Department of Electrical Engineering, Jo.C., Islamic Azad University, Jouybar, Iran, mehrdad.ahmadi@iau.ac.ir.

Received: 11.05.2026, Revised: 25.06.2026, Accepted: 19.07.2026

Abstract- This paper proposes a method to solve the optimal placement problem of DGs in distribution networks by using PSO algorithm. The formulation of bi-objective problem has been done for getting maximum benefit for DGs and distribution systems. The objective function takes into account DG owners' revenues from selling electricity and renewable energy incentives. On the other hand, distribution companies experience decreased power losses, better voltage profile, higher reliability, and environmental emissions reduction. In the evaluation of the proposed approach, simulation tests were performed in MATLAB on the IEEE 34-bus system to find the best placement and sizing of DGs. Simulation results indicate remarkable reductions in power losses, improved voltage stability, and huge economic benefits for both parties within operational limits. Thus, it was found out that the proposed PSO algorithm can be used as an efficient way of DG planning.

Keywords: Distribution networks, distributed generation, particle swarm optimization, economic benefits, generation planning.

Nomenclature

DG	Distributed Generation	EV	Electric Vehicle
DISCO	Distribution Company	i,j	Bus indices in the distribution system
PSO	Particle Swarm Optimization	K	Distributed generation unit index
GWO	Gray Wolf Optimization	N	Total number of buses
DE	Differential Evolution	$P_{DG,i}$	Active power generation by DG at bus (i) (kW)
GA	Genetic Algorithm	$Q_{DG,i}$	Reactive power generation by DG at bus (i) (kVAr)
ACO	Ant Colony Optimization	$S_{DG,i}$	Apparent power rating by DG at bus (i) (kVA)
PV	Photovoltaic	$P_{load,i}$	Active power consumption of load at bus (i) (kW)
$Q_{load,i}$	Reactive power consumption of load at bus (i) (kVAr)	R_{DG}	Revenue due to DG generation ($)
V_i	Magnitude of voltage at bus (i) (p.u.)	F_1	Objective function for the DG owner benefit

Cite this article as: M.A. Kamarposhti, P. Nouri, and M. Jalilirad, “Optimal Distributed Generation Planning Using PSO Algorithm for Economic Benefits of DG Owners and Distribution Companies,” *Artificial Intelligence Research and Applications (AIra)*, Vol. 2, No. 3, pp. 174–185, September, 2026, https://doi.org/10.20508/9e7wg123.

V_{min}	Minimum voltage limit (p.u.)
V_{max}	Maximum voltage limit (p.u.)
I_{ij}	Current between buses (i) and (j) (A)
R_{ij}	Resistance of line (i-j) (Ω)
X_{ij}	Reactance of line (i-j) (Ω)
P_{loss}	Total of active power loss (kW)
Q_{loss}	Total of reactive power loss (kVAr)
B_{DG}	Benefit of the DG owner ($)
B_{DISCO}	Benefit of the distribution company ($)
C_{DG}	Cost of DG ($)
C_{loss}	Cost of network losses ($)
F_2	Objective function or the distribution company benefit
F	Total bi-objective optimization function
ω	Inertia weight of PSO
c_1	Cognitive constant coefficient
c_2	Social constant coefficient
r_1, r_2	Random numbers in the range [0,1]
v_i	Velocity of particle i
x_i	Position of particle i
P_{best}	Best position of a particle
G_{best}	Best position found by the swarm

1. Introduction

The increasing integration of DG into current distribution systems has presented new possibilities to enhance the efficiency, reliability, and economic performance of the system. The effectiveness of the use of DG technology is highly dependent upon choosing proper locations and sizes for the DG units. Thus, optimal planning of DG has been identified as an essential research area and has been receiving much interest among scientists and utility companies. Numerous researches have been done to solve planning, control, and optimization problems in DG systems.

Hafez and Bhattacharya [1] have contributed to the study of optimally designing renewable energy power systems for microgrids. Katiraei et al. [2] have studied the independent operation of microgrids under the islanded mode, and A control strategy for voltages in distribution networks with distributed generation has been proposed by Madureira and Lopes [3]. Chowdhury et al. [4] have investigated operation and control of distributed generation power islands in smart grid. Molina and Mercado [5] used superconducting magnetic energy storage to enhance the power flow stability, while Ashabani and Mohamed [6] came up with a versatile control system for grid-tied and autonomous microgrids. Xiong and Ouyang [7] investigated modeling and transient analysis of microgrids. Alobeidli et al. [8] developed a coordinated voltage control system for hybrid microgrids. Liu et al. [9] proposed a coordinated control system for AC/DC hybrid microgrids.

Many researchers have contributed to the area of converter controls and stability analyses. Studies by Kakigano et al. [10] have been conducted on low voltage DC microgrids, Mahmoodi et al. [11] have worked on the design of power transfer control scheme for DC microgrids, while Rocabert et al. [12] have summarized the control schemes of power converters in AC microgrids. Dynamic modeling and stability-related work include Ekanayake et al. [13], Morren and De Haan [14], Coelho et al. [15], Berggren et al. [16], Guerrero et al. [17], and Lee and Wang [18], who have modeled inverters, wind generators, and small signal stability of renewable energy microgrids.

Pogaku et al. [19] examined autonomous inverter-based microgrids, and Liang and Zhuang [20] provided a review on stochastic modeling and optimization approaches. Lopes et al. [21,22] have covered the topic of distributed generation and control schemes in microgrids. Kawachi et al. [23], Basak et al. [24], and Kavousi-Fard [25] investigated power management and energy storage approaches. Zeineldin et al. [26] studied the effect of DG interface control on islanding detection, while Lidula and Rajapakse [27] conducted a review of experimental microgrids. De Brabandere et al. [28], Katiraei and Iravani [29], Barklund et al. [31], Majumder et al. [32], and Bevrani and Shokoohi [33] studied droop control and power-sharing strategies. Pan and Das [30] proposed optimization-based PID tuning for AVR systems.

Additional studies addressed machine modeling, optimization, and robust control. Freitas et al. [34] compared synchronous and induction machines for DG applications, Logenthiran et al. [35] applied evolutionary optimization for microgrid sizing, and Hossain et al. [36] proposed robust power-sharing control for low-inertia microgrids.

Studies on voltage regulation of microgrids were carried out by Vandoorn et al. [37,41], and the use of hybrid fuel cell microgrids was studied by San Martín et al. [38]. Microgrid issues were discussed by Govardhan and Roy [39], and the PV-wind-diesel hybrid system was investigated by Arulampalam et al. [40]. Kim et al. [42] and Ghazanfari et al. [43] suggested energy storage coordination and active power management schemes.

Metaheuristic algorithms have seen an increasing trend of application in optimal placement and sizing of distributed generation in recent times. Bouchikhi et al. [44] suggested a new approach to the GWO optimization algorithm in the context of optimal placement and sizing of the DG. Rajakumar et al. [45] applied Jellyfish Search Algorithm (JSA) in their research and found out the optimal placement and sizing of DGs from the perspective of PV systems and made noteworthy power losses and voltage deviations. Malika et al. [46] presented the quasi-opposition forensic algorithm-based investigation scheme for DG sizing and placement, which was found superior to other techniques.

In addition to that, Rajakumar et al. [47] introduced Osprey Optimization Algorithm (OOA) for DG placement in radial distribution systems, which proved to be very effective in minimizing power losses and improving voltage profile.

A multi-objective optimization approach [48] was recently proposed for the joint placement of distributed generators and shunt capacitors in radial distribution systems using MOPSO technique. Recently, Mohamed et al. [49] have proposed a methodology based on network partitioning for joint placement of distributed generation and electric vehicles charging stations in active distribution networks.

Table 1 indicates that most existing studies consider technical optimization objectives while the new proposed approach considers economic benefits for DG owners as well as the distribution company.

From the reviewed literature, it is evident that much work has been carried out on the control of microgrids, increasing their stability, improving their energy management systems, and integrating the distributed generation units into current distribution networks. Moreover, several optimization algorithms like GA, PSO, ACO, and DE have been applied to the planning and operation of the distributed generation.

Table 1. Comparative analysis of representative studies on DG planning and optimization.

Ref.	Method/Approach	Main Focus	Economic Consideration	Dual Economic Benefits
[1]	Renewable energy planning	Optimal microgrid supply system design	Partial	No
[3]	Coordinated voltage support	DG integration and voltage regulation	No	No
[20]	Stochastic optimization review	Microgrid optimization methods	Partial	No
[21]	DG integration framework	DG integration challenges and opportunities	No	No
[35]	Evolutionary Strategy	Optimal microgrid sizing	Partial	No
[44]	Modified GWO	DG placement and sizing	Partial	No
[45]	Jellyfish Search Algorithm	PV-DG allocation and loss reduction	No	No
[46]	Forensic-Based Investigation Algorithm	DG sizing and allocation optimization	No	No
[47]	Osprey Optimization Algorithm	DG integration and power loss minimization	No	No
[48]	MOPSO	Simultaneous DG and capacitor allocation	Partial	No
[49]	Modified Newman Fast Algorithm	DG and EV charging station planning	Partial	No

These methods have included PSO, which has proved to be one of the best techniques because of its ease, efficiency, and ability to solve nonlinear optimization problems. So far, most of the studies conducted have been done considering the goals of reducing power loss, improving voltage profiles, increasing reliability, and maximizing benefits either for DG owners or distribution companies.

However, insufficient efforts have been paid to the creation of an integrated planning model that would take into account both the interests of investors and the utility. Such a problem is especially relevant for today's intelligent distribution grids, when finding a compromise between the interests of both parties becomes crucial.

To address this issue, the present study proposes a PSO-based bi-objective optimization framework for determining the optimal location and capacity of DG units in distribution systems. The proposed model integrates the economic benefits of DG owners and the operational benefits of distribution companies while satisfying practical network constraints. The effectiveness of the proposed approach is evaluated through simulations on the IEEE 34-bus distribution system using MATLAB.

The rest of this paper is organized as follows. Section 2 presents the proposed PSO-based method, Section 3 describes the mathematical formulation, Section 4 discusses the case study and simulation results, and Section 5 concludes the paper.

2. Proposed PSO-Based Optimization Method

Based on the research gap identified in the previous section, the proposed PSO-based optimization method is presented in this section. In 1995, Kennedy and Eberhart, inspired by the collective movement of birds or schools of fish, as illustrated in Figure 1, developed the Particle Swarm Optimization (PSO) algorithm for finding optimal solutions.

Fig. 1. Biological inspiration of PSO algorithm.

The algorithm, also known as the Particle Swarm Optimization (PSO) algorithm or the Bird Algorithm, is one of the successful algorithms in the field of continuous and discrete optimization. Compared to other evolutionary algorithms, the advantages of the PSO algorithm include:

- Clear and intuitive algorithm concepts
- Simple implementation mechanism
- Ability to control and adjust its parameters
- Low memory requirements
- Capability for global random search across the entire problem space

In view of the above benefits, PSO algorithm has gained significant attention for solving various optimization problems in power systems. The PSO algorithm consists of particles that move within the search space, where each particle retains its best personal experience, including its position vector and velocity vector. Additionally, the entire particle swarm collectively builds and maintains the best collective experience.

Suppose X and Velocity represent the position and velocity vectors of the particles in a search space, respectively. Therefore, the i_{th} member of the swarm in an n-dimensional space can be described by the following two characteristics.

$$X_i = [x_{i,1}, x_{i,2}, \dots, x_{i,n}] \tag{1}$$

$$Velocity_i = [v_{i,1}, v_{i,2}, \dots, v_{i,n}] \tag{2}$$

In this algorithm, what is referred to as the velocity vector is actually determined by three factors: the velocity from the previous step, the best personal experience, and the best collective experience. These factors are updated to calculate the next velocity. The next velocity is obtained using the following relationship:

$$\begin{aligned} Velocity_i^{k+1} = \omega * Velocity_i^k + c_1 * rand(.) \\ * (P_{best,i} - X_i^k) + c_2 * rand(.) \\ * (G_{best} - X_i^k) \end{aligned} \tag{3}$$

The position vector obtains its new location through the following relationship:

$$X_i^{k+1} = Velocity_i^{k+1} + X_i^k \tag{4}$$

where ω denotes the inertia weight, c_1 and c_2 denote the learning factors, and *rand(.)* denotes a randomly generated number between 0 and 1. Additionally, k represents the current iteration number. Figure 2 represents the basic principle of operation of the PSO algorithm.

Although there are several benefits of PSO, the effectiveness of this technique is highly dependent on the settings of its parameters and it usually falls into a local optimum and quick convergence problem. The settings of the parameters of PSO algorithm adopted in this study are presented in Table 2.

The above-mentioned settings of the parameters have been established based on well-accepted guidelines of previous DG planning researches, and their effectiveness was confirmed by preliminary simulation tests.

3. Mathematical Modelling of the DG Planning Problem

Once the optimization technique is defined, the mathematical model, objectives, and operational constraints will be defined. In this research, the DG units are considered as dispatchable DGs connected to the grid. The DG units will produce an amount of active power according to the operational constraints of the system. The power values are expressed in kW, the energy values in kWh, and the economical values in USD ($). The economic assumptions are made in this research as shown in the objective function and parameters.

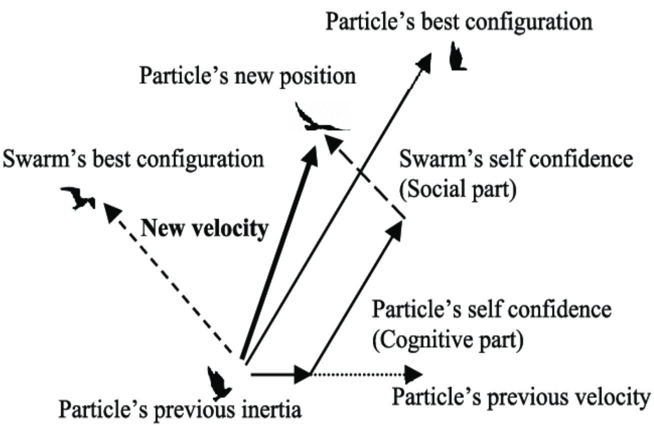

Fig. 2. Fundamental operation of the PSO algorithm.

Table 2. The parameter settings of the PSO algorithm.

Parameter	Symbol	Value
Swarm size	N	30
Maximum iterations	$Iter_{max}$	100
Inertia weight	w	0.7
Cognitive coefficient	c_1	2.0
Social coefficient	c_2	2.0
Random coefficients	r_1, r_2	[0,1]

The considered cost function consists of two parts. The first part is the profit of independent producers, which must be maximized. The second part pertains to the profit of distribution network owners, which also needs to be maximized.

$$\max J = \max[B_{IPS}, B_{DisCo}] \tag{5}$$

These weights were indicative of the level of priority given to the objective functions pertaining to the DG providers and the distribution company. Equal weight was chosen for this case to make a balanced comparison of both parties' gain.

3.1. Economic Objective for DG Owners

For the producers and owners of the Distributed Generation (DG), the cost-to-profit ratio can be described as the ratio of the annual profit to the annual cost of Distributed Generation (DG). This profit includes the revenue gained from selling the electrical energy produced as well as the incentive earned from the use of renewable energy by the government. The aforementioned cost includes the investment cost, maintenance cost, and fuel cost.

$$B_{IPS} = \frac{B_{ANN}}{C_{INV}} \tag{6}$$

$$B_{ANN} = 8760\sum_{i=1}^{N}(\rho_{DGi} + \rho_{APi})P_i^{rate}CF_i \tag{7}$$

$$C_{INV} = \sum_{i=1}^{N}\alpha_{DGi} * P_i^{rated} * C_i^{fixed} + 8760\sum_{i=1}^{N}C_i^{op} * P_i^{rated} * CF_i \tag{8}$$

where, B_{ANN} is the average annual investment profit and C_{INV} is the annual investment cost.

3.2. Economic Benefits for Distribution Companies

This benefit is divided into several components. Reduction of losses, improvement of voltage, mitigation of environmental issues, and enhancement of reliability are among the factors contributing to this benefit.

$$B_{DisCo} = \Delta B_{Ploss} + \Delta B_{Impu} + \Delta B_{Reli} + \Delta B_{Upda} + \Delta B_{Envi} + \Delta B_{Sub} \tag{9}$$

3.2.1. Benefit from power loss reduction

The total losses are decreased by using the concept of Distributed Generation (DG) in the grid network. This annual profit is calculated as follows.

$$\Delta B_{Ploss} = \rho_{GP}\Delta P_{loss}\tau_{\max} \tag{10}$$

This relationship consists of three parameters. The first parameter is the price of purchased energy. The second parameter is the difference in power losses before and after the installation of DG. The third parameter is the number of hours during which the maximum load is present in the network.

3.2.2. Benefit from voltage profile improvement

The quality of power delivered to the consumer is of great importance, and failure to comply with its standards will result in penalties. Additionally, poor power quality can reduce the lifespan of consumer devices. The formula for calculating the annual profit derived from improving the voltage profile is provided below.

$$\Delta B_{Impu} = \sum_{j\in\Phi}(\lambda_{wj} - \lambda_{woj})B_{jmu} \tag{11}$$

$$\lambda_j = \begin{cases} 1 & V_j^{rated}(1-\alpha) \leqslant V_j \leqslant V_j^{rated}(1+\alpha) \\ 0 & \text{others} \end{cases} \tag{12}$$

where λ is a binary number, B_{jmu} and the annual revenue derived from improving power quality benefits both the producer and the consumer.

3.2.3. Benefit from reliability enhancement

The use of DG in islanded systems can improve the reliability of the loads in situations where automatic sectionalizing and recloser switches operate, as well as reduce the extent of damage caused to the network due to faults occurring in one-phase. It means that the availability of DG can mitigate a part of the cost suffered due to presence of excess power in the distribution network. The costs of missing energy represent the costs incurred due to power outage or load shedding of the customers.

$$\Delta B_{Reli} = \rho_{uc} * (EENS_{woi} - EENS_{wi}) \tag{13}$$

$$EENS = \sum_{i=1}^{n}(\lambda_i * T_i * P_i) \tag{14}$$

where EENS refers to the "Expected Energy Not Supplied", ρ_{uc} refers to the cost of "expected unsupplied energy", λ_i refers to the load failure rate, n refers to the number of nodes within the independent island, T_i refers to the average time for faults, and P_i refers to the load in the independent island.

3.2.4 Benefit from network capacity improvement

The addition of distributed generation (DG) in the grid reduces the power flow in the lines, and this helps in transmitting high power.

$$\Delta B_{Upda} = \sqrt{3}C_{mar}U_{av}\sum_{i=1}^{N_b}(|I_{wi} - I_{woi}|) \tag{15}$$

where C_{mar} is the annual investment for the modernization of transmission lines. U_{av} is the average network voltage. I_w is the line current before and after the installation of DG.

3.2.5. Environmental benefits

By installing DG, transmission power losses can be reduced. Additionally, power can be generated in a distributed manner, resulting in lower and more dispersed pollution. The annual profit derived from these environmental benefits can be calculated as follows.

$$\Delta B_{Evin} = (E_{woi} - E_{wi})C_{Envi}\beta \tag{16}$$

where E_w represents total amount of electricity purchased annually from the main grid. β represents the amount of C_{O2} produced per kilowatt-hour of electrical power generation. C_{Envi} represents the tax rate for C_{O2} emissions.

3.3. Renewable Energy Incentive Benefits

The cost of power produced by renewable sources of energy is relatively high compared to non-renewable sources. However, the government encourages the use of renewable energy through incentives.

The annual profit from this component is calculated as follows.

$$\Delta B_{Sub} = \rho_{GP}(E_{woi} - E_{wi}) - 8760\sum_{i=1}^{N}\rho_{DGi}P_i^{rate}CF_i \tag{17}$$

3.4. Operational Constraints

After achieving these objectives, certain conditions must be evaluated. These constraints include simple factors that are essential for network stability.

The result obtained from the optimization algorithm must satisfy the power equations as follows.

$$P_{sub} + \sum_{i=1}^{N}P_{DGi} = P_{Loss} + P_{Load} \tag{18}$$

The voltage limit is between 0.95 and 1.05 per unit. The power electricity transmitted in the line must not exceed the maximum limit of the capacity of the line.

From the details provided in the above section, the flowchart of the algorithm will be as illustrated in Figure 3.

4. Case Study and Simulation Setup

To validate the effectiveness of the proposed technique, simulation studies have been carried out using IEEE 34-bus distribution system with various configurations of DGs. In this paper, the IEEE 34-bus distribution system is employed (Figure 4).

The network operating constraints were selected according to standard distribution system requirements. DG capacities were limited based on the loading level of the IEEE 34-bus test system. These constraints ensure practical and technically feasible DG installation scenarios throughout the optimization process. The line data and the production and consumption of buses are presented in Tables 3 and 4, respectively.

By executing the simulation program, which is coded in MATLAB, the algorithm determines the optimal buses and production values for installation based on the cost function and the described constraints. The outcomes of the algorithm are given in Table 5.

Subsequently, by simulating the installation of the obtained DGs, voltage drop and power losses are evaluated.

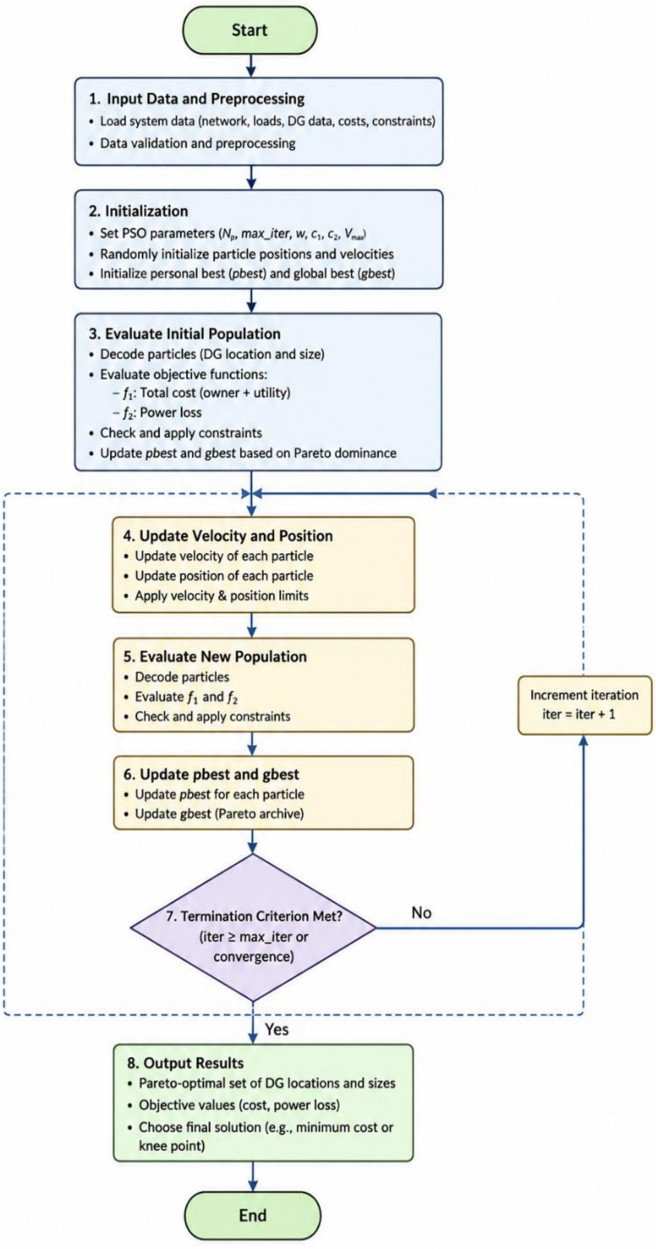

Fig. 3. Flowchart for the proposed PSO-based multi-objective optimization model.

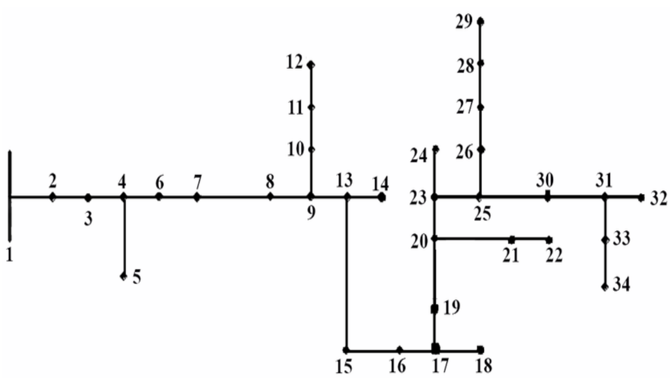

Fig. 4. IEEE standard 34-bus system.

Table 3. Consumer load data of the IEEE 34-bus system.

Bus No.	Voltage (p.u.)	Active Load (MW)	Reactive Load (MVAr)
1	1	0	0
2	1	1.7	1.12
3	1	0	0
4	1	0.0015	0.0009
5	1	0.0012	0.0008
6	1	0.033	0.04
7	1	0.0004	0.0002
8	1	0	0
9	1	0.0015	0.0009
10	1	0.04	0.026
11	1	0.02	0.0125
12	1	0.0018	0.0011
13	1	0	0
14	1	0	0
15	1	0.1713	0.1132
16	1	0	0
17	1	0.0035	0.0022
18	1	0.002	0.0012
19	1	0.015	0.0096
20	1	0.0022	0.0014
21	1	0.0064	0.004
22	1	0.218	0.149
23	1	0	0
24	1	0	0
25	1	0.0008	0.0005
26	1	0.0345	0.0222
27	1	0.0011	0.0002
28	1	0.0002	0.0001
29	1	0.002	0.0012
30	1	0	0
31	1	0.0795	0.0505
32	1	0	0
33	1	0.0041	0.0026
34	1	0.4569	0.2973

Table 4. Line parameters of the IEEE 34-bus system.

From Bus	To Bus	Resistance, R (p.u.)	Reactance, X (p.u.)
1	2	0.035	0.035
2	3	0.079	0.079
3	4	0.146	0.146
4	5	0.1406	0.1406
5	6	0.0195	0.0195
6	7	0.128	0.128
7	8	0.0216	0.0216
8	9	0.374	0.374
9	10	0.1543	0.1543
10	11	0.1439	0.1439
11	12	0.0325	0.0325
12	13	0.1191	0.1191
13	14	0.1219	0.1219
14	15	0.5622	0.5622
15	16	0.024	0.024
16	17	0.1158	0.1158
17	18	0.039	0.039
18	19	0.0135	0.0135
20	21	0.0856	0.0856
21	22	0.1843	0.1843
22	23	0.0979	0.0979
23	24	0.0946	0.0946
24	25	0.0025	0.0025
25	26	0.033	0.033
26	27	0.299	0.299
27	28	0.0449	0.0449
28	29	0.0232	0.0232
29	30	0.1367	0.1367
30	31	0.62	0.62
31	32	0.0413	0.0413
32	33	0.3021	0.3021
33	34	0.0824	0.0824

Table 5. Optimal DG placement results obtained by PSO.

Case	DG Capacity (kW)	Optimal Bus Location
1	254	13
2	300	13
3	149	13
4	143	10
5	91	8
6	47	16
7	49	4

4.1. Scenario 1: DG Installation at Bus 13 (245 kW)

In this scenario, the producer's profit is calculated as 364 USD, and the annual profit of the distribution network is obtained as 419,345 USD. Figure 5 illustrates the per-unit voltage of the buses, and Figure 6 shows the active power losses.

Figures 5 and 6 show that the installation of a 245 kW DG unit at Bus 13 enhances the voltage profile and decreases the active power loss in the distribution system.

4.2. Scenario 2: DG Installation at Bus 4 (49 kW)

In this scenario, the producer's profit is calculated as 8,387 USD, and the annual profit of the distribution network is obtained as 58,708,398 USD. Figure 7 illustrates the per-unit voltage of the buses, and Figure 8 shows the active power losses.

Figures 7 and 8 indicate that the 49 kW DG unit installed at Bus 4 maintains acceptable voltage levels while contributing to power loss reduction.

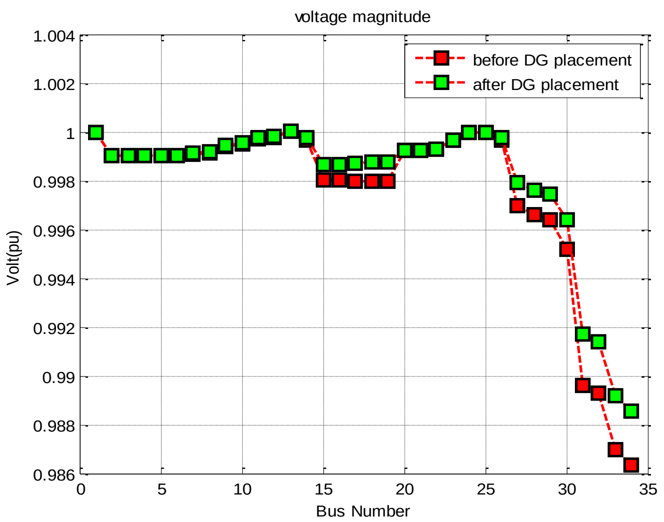

Fig. 5. Per-unit voltage of the buses in scenario 1.

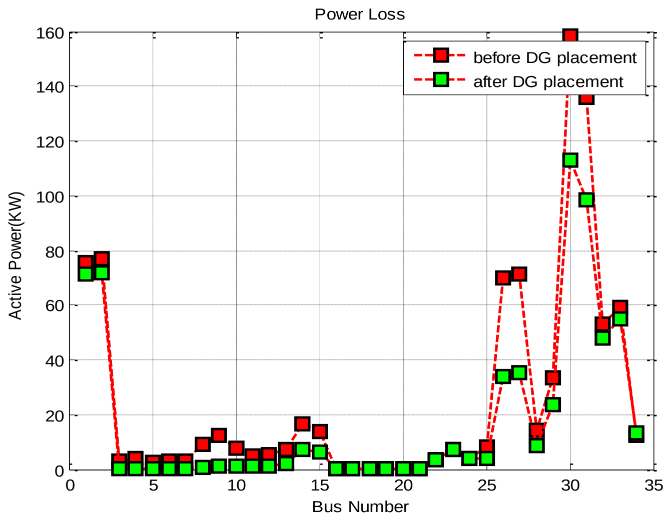

Fig. 6. Active power losses in scenario 1.

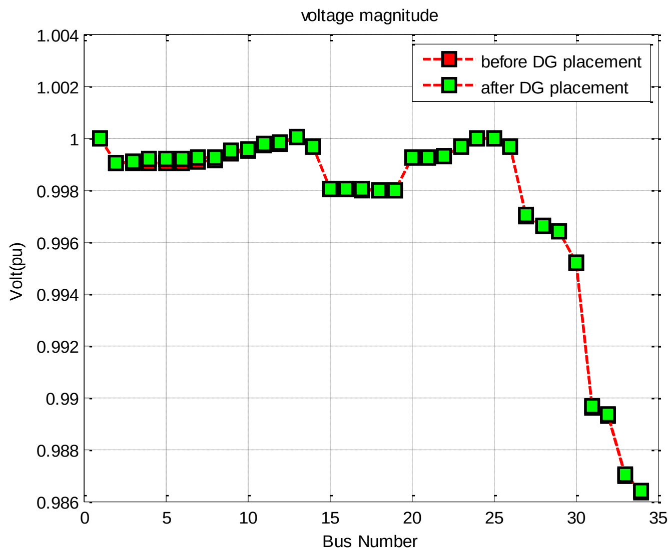

Fig. 7. Per-unit voltage of the buses in scenario 2.

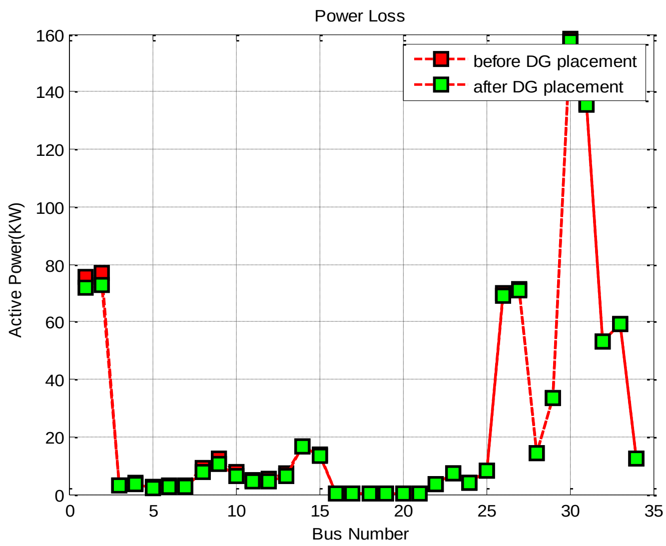

Fig. 8. Active power losses in scenario 2.

4.3. Scenario 3: DG Installation at Bus 10 (140 kW)

In this scenario, the producer's profit is calculated as 3,355 USD, and the annual profit of the distribution network is obtained as 167,738 USD. Figure 9 shows the voltage for each bus, while Figure 10 depicts active power loss.

It is clear from Figures 9 and 10 that the installation of the 140 kW DG generator at Bus 10 improves voltage profile and reduces active power loss.

4.4. Results and Discussion

This section discusses the results of the optimization process and provides a comparison between the PSO, GA, DE and GWO algorithms. Table 6 shows a comparative analysis between the suggested PSO approach to GA, DE and GWO approaches for solving DG planning problem.

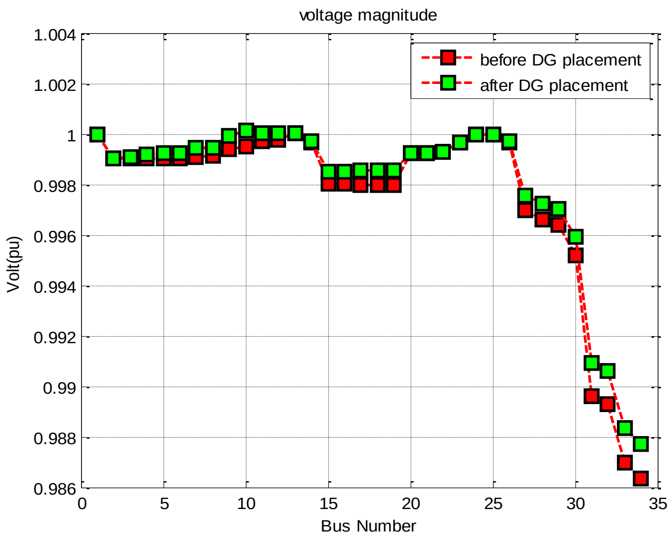

Fig. 9. Per-unit voltage of the buses in scenario 3.

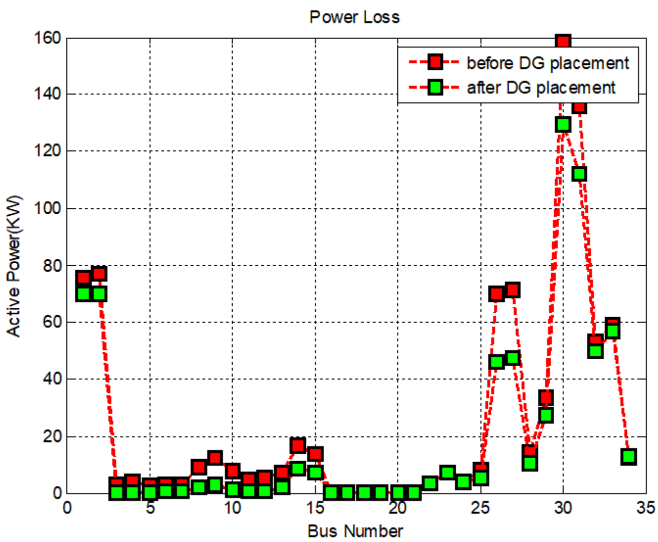

Fig. 10. Active power losses in scenario 3.

Table 6. Comparative performance of algorithms

Method	Optimal DG Size (kW)	Optimal Bus	Objective Function Value ($/year)	CPU Time (s)
GA	286	12	57,842,100	11.8
DE	291	13	58,105,420	9.7
GWO	295	13	58,314,500	8.6
PSO	300	13	58,716,785	6.9

To guarantee the statistical accuracy of the results, all the optimization approaches were run 30 times under the same settings. The best results are listed below in order to demonstrate the effectiveness of the proposed PSO algorithm in comparison with GA, DE and GWO. The PSO algorithm provided the best value of the objective function and spent the least amount of time for the calculation. Moreover, the optimal bus location provided by the PSO is the same as that of the GWO approach but with more economic advantages.

5. Conclusion

The developed algorithm in this study provided an optimization framework for the planning of distributed generations based on PSO algorithm with two objectives that provide economic advantages to DG owners as well as distribution companies. To prove the effectiveness of the developed technique, simulation results were provided for IEEE 34-bus distribution system taking into consideration all operational constraints. It is seen from these simulation results that power losses were reduced significantly and the economic advantage was increased along with the improvement of voltage profiles without violating operating limits. This proves that the PSO-based planning technique introduced in this work is a promising and feasible solution for DG planning problem.

Author Contributions

M.A.K. conceptualized the study, developed the methodology and software, performed the validation, formal analysis, and investigation, contributed to the resources and data curation, prepared the original draft of the manuscript, reviewed and edited the manuscript, performed the visualization, supervised the research, and administered the project; P.N. contributed to the conceptualization, methodology, software development, validation, formal analysis, investigation, resources, and data curation, prepared the original draft of the manuscript, reviewed and edited the manuscript, and performed the visualization; M.J. contributed to the conceptualization, methodology, software development, validation, formal analysis, investigation, resources, and data curation, prepared the original draft of the manuscript, reviewed and edited the manuscript, performed the visualization, supervised the research, and administered the project. All authors have read and approved the final version of the manuscript.

Acknowledgements

Not applicable.

Conflict of Interest

The authors declare no conflict of interest.

References

[1] O. Hafez and K. Bhattacharya, "Optimal planning and design of a renewable energy based supply system for microgrids," *Renewable Energy*, vol. 45, pp. 7–15, 2012, doi: 10.1016/j.renene.2012.01.087.

[2] F. Katiraei, M. R. Iravani, and P. W. Lehn, "Micro-grid autonomous operation during and subsequent to islanding process," *IEEE Transactions on Power Delivery*, vol. 20, no. 1, pp. 248–257, 2005, doi: 10.1109/TPWRD.2004.835051.

[3] A. G. Madureira and J. A. Peças Lopes, "Coordinated voltage support in distribution networks with distributed generation and microgrids," *IET Renewable Power Generation*, vol. 3, no. 4, pp. 439–454, 2009, doi: 10.1049/iet-rpg.2008.0064.

[4] S. P. Chowdhury, S. Chowdhury, C. F. Ten, and P. A. Crossley, "Operation and control of DG based power island in smart grid environment," *20th International Conference and Exhibition on Electricity Distribution (CIRED 2009)*, Prague, Czech Republic, p. 1051, 2009, doi: 10.1049/cp.2009.0565.

[5] M. G. Molina and P. E. Mercado, "Power flow stabilization and control of microgrid with wind generation by superconducting magnetic energy storage," *IEEE Transactions on Power Electronics*, vol. 26, no. 3, pp. 910–922, 2011, doi: 10.1109/TPEL.2010.2097609.

[6] S. M. Ashabani and Y. A.-R. I. Mohamed, "A flexible control strategy for grid-connected and islanded microgrids with enhanced stability using nonlinear microgrid stabilizer," *IEEE Transactions on Smart Grid*, vol. 3, no. 3, pp. 1291–1301, 2012, doi: 10.1109/TSG.2012.2202131.

[7] X. Xiong and J. Ouyang, "Modeling and transient behavior analysis of an inverter-based microgrid," *Electric Power Components and Systems*, vol. 40, no. 1, pp. 112–130, 2011, doi: 10.1080/15325008.2011.629333.

[8] K. A. Alobeidli, M. H. Syed, M. S. El Moursi, and H. H. Zeineldin, "Novel coordinated voltage control for hybrid micro-grid with islanding capability," *IEEE Transactions on Smart Grid*, vol. 6, no. 3, pp. 1116–1127, 2015, doi: 10.1109/TSG.2014.2377155.

[9] X. Liu, P. Wang, and P. C. Loh, "A hybrid AC/DC microgrid and its coordination control," *IEEE Transactions on Smart Grid*, vol. 2, no. 2, pp. 278–286, 2011, doi: 10.1109/TSG.2011.2116162.

[10] H. Kakigano, Y. Miura, and T. Ise, "Low-voltage bipolar-type DC microgrid for super high quality distribution," *IEEE Transactions on Power Electronics*, vol. 25, no. 12, pp. 3066–3075, 2010, doi: 10.1109/TPEL.2010.2077682.

[11] M. Mahmoodi, R. Noroozian, G. B. Gharehpetian, and M. Abedi, "A suitable power transfer control system for interconnection converter of DC microgrids," *Renewable Energy and Power Quality Journal*, vol. 1, no. 6, 2008, doi: 10.24084/repqj06.318.

[12] J. Rocabert, A. Luna, F. Blaabjerg, and P. Rodriguez, "Control of power converters in AC microgrids," *IEEE Transactions on Power Electronics*, vol. 27, no. 11, pp. 4734–4749, 2012, doi: 10.1109/TPEL.2012.2199334.

[13] J. B. Ekanayake, L. Holdsworth, X. Wu, and N. Jenkins, "Dynamic modeling of doubly fed induction generator wind turbines," *IEEE Transactions on Power Systems*, vol. 18, no. 2, pp. 803–809, 2003, doi: 10.1109/TPWRS.2003.811178.

[14] J. Morren and S. W. H. de Haan, "Ride-through of wind turbines with doubly-fed induction generator during a voltage dip," *IEEE Transactions on Energy Conversion*, vol. 20, no. 2, pp. 435–441, 2005, doi: 10.1109/TEC.2005.845526.

[15] E. A. A. Coelho, P. C. Cortizo, and P. F. D. Garcia, "Small-signal stability for parallel-connected inverters in stand-alone AC supply systems," *IEEE Transactions on Industry Applications*, vol. 38, no. 2, pp. 533–542, 2002, doi: 10.1109/28.993176.

[16] B. Berggren, R. Majumder, and N. Johansson, "A generic VSC HVDC primary control structure suitable for stability studies," *2013 EPRI HVDC & FACTS Conference*, pp. 1–8, 2013.

[17] J. M. Guerrero, L. G. de Vicuña, J. Matas, M. Castilla, and J. Miret, "A wireless controller to enhance dynamic performance of parallel inverters in distributed generation systems," *IEEE Transactions on Power Electronics*, vol. 19, no. 5, pp. 1205–1213, 2004, doi: 10.1109/TPEL.2004.833451.

[18] D. J. Lee and L. Wang, "Small-signal stability analysis of an autonomous hybrid renewable energy power generation/energy storage system part I: Time-domain simulations," *IEEE Transactions on Energy Conversion*, vol. 23, no. 1, pp. 311–320, 2008, doi: 10.1109/TEC.2007.914309.

[19] N. Pogaku, M. Prodanovic, and T. C. Green, "Modeling, analysis and testing of autonomous operation of an inverter-based microgrid," *IEEE Transactions on Power Electronics*, vol. 22, no. 2, pp. 613–625, 2007, doi: 10.1109/TPEL.2006.890003.

[20] H. Liang and W. Zhuang, "Stochastic modeling and optimization in a microgrid: A survey," *Energies*, vol. 7, no. 4, pp. 2027–2050, 2014, doi: 10.3390/en7042027.

[21] J. P. Lopes, N. Hatziargyriou, J. Mutale, P. Djapic, and N. Jenkins, "Integrating distributed generation into electric power systems: A review of drivers, challenges and opportunities," *Electric Power Systems Research*, vol. 77, no. 9, pp. 1189–1203, 2007, doi: 10.1016/j.epsr.2006.08.016.

[22] J. P. Lopes, C. L. Moreira, and A. G. Madureira, "Defining control strategies for microgrids islanded operation," *IEEE Transactions on Power Systems*, vol. 21, no. 2, pp. 916–924, 2006, doi: 10.1109/TPWRS.2006.873018.

[23] S. Kawachi, J. Baba, T. Kikuchi, E. Shimoda, S. Numata, E. Masada, and T. Nitta, "State of charge control for energy storage by use of cascade control system for microgrid," *2009 International Conference on Clean Electrical Power*, Capri, Italy, pp. 370–375, 2009, doi: 10.1109/ICCEP.2009.5212057.

[24] P. Basak, S. Chowdhury, S. H. nee Dey, and S. P. Chowdhury, "A literature review on integration of distributed energy resources in the perspective of control, protection and stability of microgrid," *Renewable and Sustainable Energy Reviews*, vol. 16, no. 8, pp. 5545–5556, 2012, doi: 10.1016/j.rser.2012.05.043.

[25] A. Kavousi-Fard, "A new fuzzy-based feature selection and hybrid TLA–ANN modelling for short-term load forecasting," *Journal of Experimental & Theoretical Artificial Intelligence*, vol. 25, no. 4, pp. 543–557, 2013, doi: 10.1080/0952813X.2013.782348.

[26] H. H. Zeineldin, E. F. El-Saadany, and M. M. A. Salama, "Impact of DG interface control on islanding detection and nondetection zones," *IEEE Transactions on Power Delivery*, vol. 21, no. 3, pp. 1515–1523, 2006, doi: 10.1109/TPWRD.2005.858173.

[27] N. W. A. Lidula and A. D. Rajapakse, "Microgrids research: A review of experimental microgrids and test systems," *Renewable and Sustainable Energy Reviews*, vol. 15, no. 1, pp. 186–202, 2011, doi: 10.1016/j.rser.2010.09.041.

[28] K. De Brabandere, B. Bolsens, J. Van den Keybus, A. Woyte, J. Driesen, and R. Belmans, "A voltage and frequency droop control method for parallel inverters," *IEEE Transactions on Power Electronics*, vol. 22, no. 4, pp. 1107–1115, 2007, doi: 10.1109/TPEL.2007.900456.

[29] F. Katiraei and M. R. Iravani, "Power management strategies for a microgrid with multiple distributed generation units," *IEEE Transactions on Power Systems*, vol. 21, no. 4, pp. 1821–1831, 2006, doi: 10.1109/TPWRS.2006.879260.

[30] I. Pan and S. Das, "Frequency domain design of fractional order PID controller for AVR system using chaotic multi-objective optimization," *International Journal of Electrical Power & Energy Systems*, vol. 51, pp. 106–118, 2013, doi: 10.1016/j.ijepes.2013.02.021.

[31] E. Barklund, N. Pogaku, M. Prodanovic, C. Hernandez-Aramburo, and T. C. Green, "Energy management in autonomous microgrid using stability-constrained droop control of inverters," *IEEE Transactions on Power Electronics*, vol. 23, no. 5, pp. 2346–2352, 2008, doi: 10.1109/TPEL.2008.2001910.

[32] R. Majumder, B. Chaudhuri, A. Ghosh, R. Majumder, G. Ledwich, and F. Zare, "Improvement of stability and load sharing in an autonomous microgrid using supplementary droop control loop," *IEEE Transactions on Power Systems*, vol. 25, no. 2, pp. 796–808, 2010, doi: 10.1109/TPWRS.2009.2032049.

[33] H. Bevrani and S. Shokoohi, "An intelligent droop control for simultaneous voltage and frequency regulation in islanded microgrids," *IEEE Transactions on Smart Grid*, vol. 4, no. 3, pp. 1505–1513, 2013, doi: 10.1109/TSG.2013.2258947.

[34] W. Freitas, J. C. Vieira, A. Morelato, L. C. da Silva, V. F. da Costa, and F. A. Lemos, "Comparative analysis between synchronous and induction machines for distributed generation applications," *IEEE Transactions on Power Systems*, vol. 21, no. 1, pp. 301–311, 2006, doi: 10.1109/TPWRS.2005.860931.

[35] T. Logenthiran, D. Srinivasan, A. M. Khambadkone, and T. S. Raj, "Optimal sizing of an islanded microgrid using evolutionary strategy," *2010 IEEE 11th International Conference on Probabilistic Methods Applied to Power Systems*, Singapore, pp. 12–17, 2010, doi: 10.1109/PMAPS.2010.5528976.

[36] M. J. Hossain, H. R. Pota, M. A. Mahmud, and M. Aldeen, "Robust control for power sharing in microgrids with low-inertia wind and PV generators," *IEEE Transactions on Sustainable Energy*, vol. 6, no. 3, pp. 1067–1077, 2015, doi: 10.1109/TSTE.2014.2317805.

[37] T. L. Vandoorn, C. M. Ionescu, J. D. De Kooning, R. De Keyser, and L. Vandevelde, "Theoretical analysis and experimental validation of single-phase direct versus cascade voltage control in islanded microgrids," *IEEE Transactions on Industrial Electronics*, vol. 60, no. 2, pp. 789–798, 2013, doi: 10.1109/TIE.2012.2205362.

[38] J. I. San Martín, I. Zamora, J. J. San Martín, V. Aperribay, and P. Eguia, "Hybrid fuel cells technologies for electrical microgrids," *Electric Power Systems Research*, vol. 80, no. 9, pp. 993–1005, 2010, doi: 10.1016/j.epsr.2010.01.006.

[39] M. D. Govardhan and R. Roy, "Notice of violation of IEEE publication principles: A review on key issues of microgrid," *2011 IEEE PES Innovative Smart Grid Technologies-India (ISGT India)*, pp. 322–327, 2011, doi: 10.1109/ISET-India.2011.6145390.

[40] A. Arulampalam, N. Mithulananthan, R. C. Bansal, and T. K. Saha, "Micro-grid control of PV-wind-diesel hybrid system with islanded and grid connected operations," *2010 IEEE International Conference on Sustainable Energy Technologies (ICSET)*, Kandy, Sri Lanka, pp. 1–5, 2010, doi: 10.1109/ICSET.2010.5684443.

[41] T. L. Vandoorn, B. Meersman, L. Degroote, B. Renders, and L. Vandevelde, "A control strategy for islanded microgrids with DC-link voltage control," *IEEE Transactions on Power Delivery*, vol. 26, no. 2, pp. 703–713, 2011, doi: 10.1109/TPWRD.2010.2095884.

[42] J. Y. Kim, J. H. Jeon, S. K. Kim, C. Cho, J. H. Park, H. M. Kim, and K. Y. Nam, "Cooperative control strategy of energy storage system and microsources for stabilizing the microgrid during islanded operation," *IEEE Transactions on Power Electronics*, vol. 25, no. 12, pp. 3037–3048, 2010, doi: 10.1109/TPEL.2010.2073488.

[43] A. Ghazanfari, M. Hamzeh, H. Mokhtari, and H. Karimi, "Active power management of multihybrid fuel cell/supercapacitor power conversion system in a medium voltage microgrid," *IEEE Transactions on Smart Grid*, vol. 3, no. 4, pp. 1903–1910, 2012, doi: 10.1109/TSG.2012.2197832.

[44] N. Bouchikhi, F. Boussadia, R. Bouddou, A. O. Salau, S. Mekhilef, C. Gouder, S. Adiche, and A. Belabbes, "Optimal distributed generation placement and sizing using modified grey wolf optimization and ETAP for power system performance enhancement and protection adaptation," *Scientific Reports*, vol. 15, no. 1, p. 13919, 2025, doi: 10.1038/s41598-025-98012-0.

[45] P. Rajakumar, P. M. Balasubramaniam, E. Parimalasundar, K. Suresh, and P. Aravind, "Optimized placement and sizing of solar photovoltaic distributed generation using jellyfish search algorithm for enhanced power system performance," *Scientific Reports*, vol. 15, no. 1, p. 20755, 2025, doi: 10.1038/s41598-025-08227-4.

[46] B. K. Malika, V. Pattanaik, S. Panda, B. K. Sahu, P. K. Rout, M. Bajaj, V. Blazek, L. Prokop, and S. Misak, "A quasi oppositional forensic based investigation algorithm for optimizing distributed generation placement and sizing in power distribution systems," *Scientific Reports*, vol. 15, no. 1, p. 16471, 2025, doi: 10.1038/s41598-025-01378-4.

[47] P. Rajakumar, P. M. Balasubramaniam, A. Munimathan, M. Alwetaishi, M. I. Gulbarga, and C. Senthilpari, "Osprey optimization algorithm for distributed generation integration in a radial distribution system for power loss reduction," *Scientific Reports*, vol. 15, no. 1, p. 18775, 2025, doi: 10.1038/s41598-025-02411-2.

[48] P. Patel, N. Patil, A. Mohsen, A. Kashyap, N. A. Hasan, K. A., D. N. Thatoi, D. Gupta, and A. Kamranfar, "Multi-objective particle swarm optimization algorithm-based method for optimal placement and sizing of distributed generations and shunt capacitors in a radial distribution network," *Results in Engineering*, vol. 27, p. 106514, 2025, doi: 10.1016/j.rineng.2025.106514.

[49] M. A. E. Mohamed, A. N. A. Gawish, and M. E. Metwally, "Optimal electric vehicle charging stations and distributed generation placement by partitioning the distribution network using the modified Newman fast algorithm," *Scientific Reports*, vol. 16, no. 1, p. 6341, 2026, doi: 10.1038/s41598-026-35433-5.